

Fall 11-17-2018

# Design and Fabrication of FDM 3D Printed Strain Sensors

Austin Smith  
*Louisiana Tech University*

Follow this and additional works at: <https://digitalcommons.latech.edu/theses>

---

## Recommended Citation

Smith, Austin, "" (2018). *Thesis*. 4.  
<https://digitalcommons.latech.edu/theses/4>

This Thesis is brought to you for free and open access by the Graduate School at Louisiana Tech Digital Commons. It has been accepted for inclusion in Master's Theses by an authorized administrator of Louisiana Tech Digital Commons. For more information, please contact [digitalcommons@latech.edu](mailto:digitalcommons@latech.edu).

**DESIGN AND FABRICATION OF FDM 3D PRINTED  
STRAIN SENSORS**

by

Austin Smith, B.S.

A Thesis Presented in Partial Fulfillment  
of the Requirements of the Degree  
Master of Science

COLLEGE OF ENGINEERING AND SCIENCE  
LOUISIANA TECH UNIVERSITY

November 2018

LOUISIANA TECH UNIVERSITY  
THE GRADUATE SCHOOL

**SEPTEMBER 18, 2018**

Date

We hereby recommend that the thesis prepared under our supervision by  
Austin **Smith**, B.S.

entitled **Design and Fabrication of FDM 3D Printed Strain Sensors**

be accepted in partial fulfillment of the requirements for the Degree of

**Master of Science in Molecular Science and Nanotechnology**

\_\_\_\_\_  
Supervisor of Thesis Research

\_\_\_\_\_  
Head of Department

**COES**

\_\_\_\_\_  
Department

Recommendation concurred in:

\_\_\_\_\_  
\_\_\_\_\_  
\_\_\_\_\_

Advisory Committee

**Approved:**

\_\_\_\_\_  
Director of Graduate Studies

\_\_\_\_\_  
Dean of the College

**Approved:**

\_\_\_\_\_  
Dean of the Graduate School

## ABSTRACT

As technology related to virtual reality, prosthetics, and robotics advances there appears a need for better sensor technology to augment these systems. In particular, many of the systems must interphase with the human body or the environment while maintaining large amounts of mobility and flexibility. This creates the demand for flexible electronics in particular flexible strain sensors to monitor movement. The work presented here explores the feasibility of commercially available elastic filament and desktop Fused Deposition Modeling (FDM) 3D printing as a simple and cost-effective route to develop flexible single-axis strain sensors. 3D printing allows for the rapid production and prototyping of designs at relatively low cost. 3D printing is used to fabricate the strain sensor substrate. The sensitivity of the strain sensor is then observed by calculating the gauge factor from experimental data. From this, the viability of FDM 3D printing and commercially available filament for the creation of strain sensors can be determined. Three sensors measuring approximately 2100  $\mu\text{m}$  by 199  $\mu\text{m}$  are fabricated. Results demonstrate gauge factors from 1 to 2 at 38.6% strain with high linearity and little hysteresis. Additionally, two smaller strain sensors, measuring approximately 696  $\mu\text{m}$  by 203  $\mu\text{m}$ , are fabricated with gauge factors of nearly 0.9 at 13% strain. Results show that stress accumulation and permanent deformation play an essential role in determining the functionality of these 3D printed sensors. The results from this work

demonstrate the potential of additive manufacturing to produce complex designs and sensor platforms for a wide range of applications.

## APPROVAL FOR SCHOLARLY DISSEMINATION

The author grants to the Prescott Memorial Library of Louisiana Tech University the right to reproduce, by appropriate methods, upon request, any or all portions of this Thesis. It is understood that “proper request” consists of the agreement, on the part of the requesting party, that said reproduction is for his personal use and that subsequent reproduction will not occur without written approval of the author of this Thesis. Further, any portions of the Thesis used in books, papers, and other works must be appropriately referenced to this Thesis.

Finally, the author of this Thesis reserves the right to publish freely, in the literature, at any time, any or all portions of this Thesis.

Author Austin Smith

Date 09/18/2018

## TABLE OF CONTENTS

ABSTRACT.....	iii
APPROVAL FOR SCHOLARLY DISSEMINATION .....	v
LIST OF FIGURES .....	viii
LIST OF TABLES .....	x
ACKNOWLEDGMENTS .....	xi
CHAPTER 1 INTRODUCTION .....	1
1.1 Strain Sensor Overview .....	1
1.2 Motivation Behind the Work .....	3
1.3 Objective of the Work.....	3
1.4 Thesis Outline.....	4
CHAPTER 2 FABRICATION METHODS .....	5
2.1 Overview of Fabrication Methods .....	5
2.2 Molding.....	5
2.3 Coating.....	7
2.4 Contact Printing .....	9
2.5 3D Printing.....	10
CHAPTER 3 METHODS .....	13
3.1 Approach and Methods.....	13
3.2 Approach.....	13
3.3 Fabrication .....	15

3.4	Experimental Apparatus and Approach Towards Characterization of the Fabricated Strain Sensor .....	19
3.5	Characterization of Channels.....	21
3.6	Tensile Test.....	22
CHAPTER 4 RESULTS .....		24
4.1	Results Overview .....	24
4.2	Resistance VS Strain and Sensitivity Measurements .....	25
4.3	Force Displacement and Tensile Tests .....	33
4.4	Geometric Fidelity of Strain Sensor Channels .....	38
CHAPTER 5 CONCLUSIONS AND FUTURE WORK.....		43
5.1	Conclusions.....	43
5.2	Future Work.....	44
APPENDIX A RAW DATA FOR RESISTANCE VS STRAIN CHARTS .....		45
A.1	Type I Strain Sensor .....	45
A.2	Type II Strain Sensor .....	47
BIBLIOGRAPHY .....		48

## LIST OF FIGURES

<b>Figure 2-1:</b> Representative diagram of molding process used to fabricate strain sensors.....	6
<b>Figure 2-2:</b> Representative diagram of coating process used to fabricate strain sensors.....	8
<b>Figure 2-3:</b> Representative diagram of the contact printing process used to fabricate strain sensors.....	9
<b>Figure 2-4:</b> Representative Diagram of Embedded 3D printing based on Muth <i>et al.</i> procedure [2].....	11
<b>Figure 3-1:</b> Cross-sectional view of the 3D printed strain sensor design.....	14
<b>Figure 3-2:</b> Working principle of the channel effects when under applied strained.....	15
<b>Figure 3-3:</b> Design of strain sensor: a) Top view of Type I strain sensor and b) Side view of Type I channel port. c) Top view of Type II strain sensor and d) Side view of Type II channel port.....	16
<b>Figure 3-4:</b> Representative diagram outlining the strain sensor fabrication process.....	18
<b>Figure 3-5:</b> Fully fabricated and assembled strain sensor.....	19
<b>Figure 3-6:</b> Experiment setup used for characterization of the fabricated strain sensor: a) Schematic diagram of experiment setup, b) Laboratory apparatus and c) circuitry diagram used for estimating voltage drop and resistance change.....	21
<b>Figure 3-7:</b> Tensile test setup with key parts labeled.....	23
<b>Figure 4-1:</b> Resistance vs Strain Curve for Type I strain sensor Sample I.....	25
<b>Figure 4-2:</b> Resistance vs Strain Curve for Type I strain sensor Sample II.....	26
<b>Figure 4-3:</b> Resistance vs Strain Curve for Type I strain sensors Sample III.....	26
<b>Figure 4-4:</b> Tensile test process and a chart of resistance vs strain to demonstrate the effect of stress accumulation. a) Strain sensor substrate before strain b) Strain sensor substrate during strain c) Deformed strain sensor substrate due to stress accumulation d) Effect of stress accumulation on initial resistance.....	28

<b>Figure 4-5:</b> Change in resistance vs. strain for the Type II strain sensor. a) Sample IV b) Sample V. ....	30
<b>Figure 4-6:</b> Failure of Type II strain sensors a) strain sensor in testing setup under tension b) image of bottleneck that exists at the corner. c) CLS 3D image of the bottleneck observed during dimensional characterization. d) COMSOL model of stress concentrations near the corners. ....	32
<b>Figure 4-7:</b> Force-displacement curve of Type I strain Sensor out to the maximum tested strain. ....	33
<b>Figure 4-8:</b> Relaxation effects as a result of cyclic straining/unstraining of the 3D printed sensor substrate. ....	34
<b>Figure 4-9:</b> Comparison of 32.2% Force vs Strain after 3 cycles to 38.6% Force vs Strain. ....	35
<b>Figure 4-10:</b> Image of strain sensor with zoomed in image of filament fibers shown in diagonal crossing pattern with respect to applied strain. ....	36
<b>Figure 4-11:</b> Stress-strain curves obtained from tensile tests showing strain offset and stress accumulation experienced by the 3D printed samples. ....	37
<b>Figure 4-12:</b> Images of the analyzer software as it was used to measure dimensions. a) Image of Type I channel measurement process. b) Image of Type II channel measurement process. ....	39
<b>Figure A-5-1:</b> Resistance vs Displacement curve Sample I. ....	45
<b>Figure A-5-2:</b> Resistance vs Displacement curve for Sample II. ....	46
<b>Figure A-5-3:</b> Resistance vs Displacement curve for Sample III. ....	46
<b>Figure A-5-4:</b> Resistance vs Displacement curve for Sample IV. ....	47
<b>Figure A-5-5:</b> Resistance vs Displacement curve for Sample V. ....	47

## LIST OF TABLES

<b>Table 3-1:</b> Setting and parameters used to print the strain sensors using Ultimaker 3 FDM 3D printer. ....	17
<b>Table 4-1:</b> Strain, initial length, initial resistance, and calculated gauge factors for the three strain sensor samples.....	27
<b>Table 4-2:</b> Measured dimensions of 3D printed sensors.....	40
<b>Table 4-3:</b> Comparison of recently reported resistive flexible strain sensors selected from the literature. ....	41

## **ACKNOWLEDGMENTS**

I would like to thank LASPACE for assisting in funding this project. Furthermore, I would like to express my thanks to Dr.Hamzeh Bardaweel, without his guidance and help this thesis would not have been possible. I would like to thank my committee members for being available on such short notice. I would like to thank Dr. David K. Mills for being generous enough to allow me to use his tensile test machine. Last, I would like to thank my lab mate Mehdi Mofidian for assisting me with modeling and checking my figure quality.

# **CHAPTER 1**

## **INTRODUCTION**

### **1.1 Strain Sensor Overview**

In recent years there has been a growing interest in flexible electronics [1]–[3]. The main reason for this interest is the integration of flexible electronics into clothing or wearable devices that conform to the human body [4]. One of the more researched areas of flexible electronics is strain sensors as their ability to monitor changes in bodily movement makes them ideal for health monitoring, human-machine interfaces such as Virtual Reality controls, and as sensors for machine environment interface such as with robots or prosthetic limbs [1]–[5].

Currently, most of the research into flexible strain sensors is directed towards three main areas: Sensitivity (Gauge Factor), elasticity, and the fabrication process [1]. In the areas of sensitivity and elasticity, the main goal is to create a device that is both extremely sensitive and can be strained to high levels. In the area of fabrication, researchers are looking to develop cost-effective methods to fabricate flexible sensors [2]. Research also seeks to integrate multiple sensors into one device and decouple the readouts in order to monitor force in multiple directions [6].

The main difference between conventional strain sensors and flexible strain sensors lies in the amount of strain that can be measured. Conventional strain sensors

usually only have a maximum strain of around 5% while flexible strain sensors have been fabricated with maximum strains as high as 800% [1], [7]. The drastic increase in the range of measurable strains allows flexible strain sensors a wider range of possible applications when compared to the conventional ones. This, in part, is the reason for the increased interest in flexible electronics as flexible strain sensors allow for sensors to be implemented into a much wider array of devices and fields.

The sensitivity of a strain sensor is based on its Gauge Factor (GF). The GF is defined in terms of the change in the strain sensor readout whether it is capacitance, voltage, or resistance in response to applied strain. The higher the gauge factor the more sensitive the strain sensor is. The basic equation for GF is given by [8]:

$$GF = \frac{\Delta R/R_0}{\varepsilon} \quad \text{Eq. 1-1}$$

where  $\Delta R$  and  $R_0$  are the change in resistance and initial resistance respectively and  $\varepsilon$  is the strain. Conventional strain sensors tend to have relatively low elasticity and sensitivity (GF of 2 and maximum strain 5%) [7]. Nowadays, research focuses mainly on increasing the elasticity and sensitivity of the strain sensors. However, many of the strain sensors that have been developed with high gauge factors lack elasticity while the strain sensors with higher elasticity lack sensitivity [1]. A review by Amjadi *et al.* did extensive research into experimental strain sensors currently being fabricated [1]. Amjadi *et al.* showed that creating a strain sensor with gauge factor greater than 64 and elongation greater than 100% has proven challenging [1]. Nonetheless, many of the materials used to create the highly sensitive strain sensors lack flexibility or ductility [1]. Moreover, methods like crack propagation are preferred for measuring smaller strains with higher sensitivity [9]. Also, most highly flexible materials are nonconductive and, thereby, must

be integrated with conductive materials such that when they are strained a readout can be made. Methods for integrating conductive materials into elastic structures include but are not limited to the introduction and patterning of conductive nanoparticles or nanowires into or onto the flexible material, or injecting liquid conductors into microchannels that have been encapsulated in flexible material [6], [10].

## **1.2 Motivation Behind the Work**

The motivation behind this work is the desire to explore different areas in which desktop FDM 3D printing can be used to fabricate cost-effective viable sensors for health monitoring using commercial materials. 3D printing allows for fast and relatively accurate fabrication of complex designs and networks. It has the potential to allow for quick sensor fabrication on sight as well as the possibility for reduced cost in sensor production. The use of commercialized materials means that these materials are already available and tested rather than fabricating specially made materials. This allows for the production of relatively inexpensive flexible and wearable sensors which can be used for an array of health monitoring styles and systems. 3D printed flexible sensors can also be customized to fit the individual. In turn, these sensors could allow for less invasive and more patient-friendly medical care and health monitoring.

## **1.3 Objective of the Work**

The objective of this thesis is to explore the feasibility of commercially available flexible filament and desktop fused deposition modeling FDM 3D printing techniques to develop flexible strain sensors as a simple and cost-effective method of mass production. 3D printing allows for the creation of complex three-dimensional structures, rapid design iterations, decreased waste, and reduced labor and cost. To achieve the main objective of

this thesis specific milestones and goals were sought. First, single axis strain sensors were designed. Second, FDM 3D printing was used to fabricate the strain sensors. Third, an experimental apparatus was built and used to perform full characterization of the fabricated sensors. Next, a microscope was used to confirm dimensional fidelity. Last, tensile tests were performed to examine the nature of the elastic material used to form the strain sensors.

#### **1.4 Thesis Outline**

This thesis deals with design, fabrication, and characterization of 3D printed strain sensors. First, an overview of the fabrication methods used to fabricate flexible strain sensors is outlined in chapter 2. These consist of Molding (Section 2.2), Coating (Section 2.3), Contact printing (Section 2.4) and 3D Printing (Section 2.5). Next, the design and working principle of the strain sensors is described in Section 3.2. The fabrication process of the strain sensor is outlined in Section 3.3. Experimental methods used to characterize the fabricated strain sensors are described in Section 3.4. Characterization tests described in this thesis include characterization of fabricated channels (Section 3.5), and tensile testing (Section 3.6). The channel characterization subsection describes the methods used to measure and image the channel dimensions. The tensile testing subsection explains the procedure used to perform the tensile tests on the elastic substrates. Additionally, the results obtained from these tests are discussed in Sections 4.2 to 4.4. Main findings from this work are summarized in Section 5.1.

## **CHAPTER 2**

### **FABRICATION METHODS**

#### **2.1 Overview of Fabrication Methods**

There are numerous materials and methods being researched for the development of strain gauges including 3D printing, molding, Contact printing, and coating [1], [2], [4], [6]–[8], [10]–[13]. The focus of these fabrication methods is to introduce conductive materials into a flexible substrate such that changes in resistance, voltage, or capacitance can be measured accurately. The fabrication methods also focus on either increasing the functionality of the strain sensor by increasing its GF or modifying the process to make the strain sensor more cost effective and industry friendly [2]. For example, 3D printing has been proposed as a cost-effective and industry-friendly method for fabricating strain gauges with higher gauge factors.

#### **2.2 Molding**

Molding is a multi-step process by which the strain sensors are fabricated. Typically, molding is done by creating a sacrificial structure that is then cast inside of a liquid elastomer [8]. The liquid elastomer is then allowed to cure. After the curing process the sacrificial structure is etched away and the mold is sealed using another layer of the cured elastomer over the top [8]. This is followed by an injection process. An example of the molding process used to fabricate strain sensors is outlined in Figure 2-1.

A major advantage of using the molding process is that it allows for the use of diverse elastic materials as well as a variety of techniques to produce channels of different sizes and structures. Additionally, molding also allows for the use of a variety of conductive fillers.

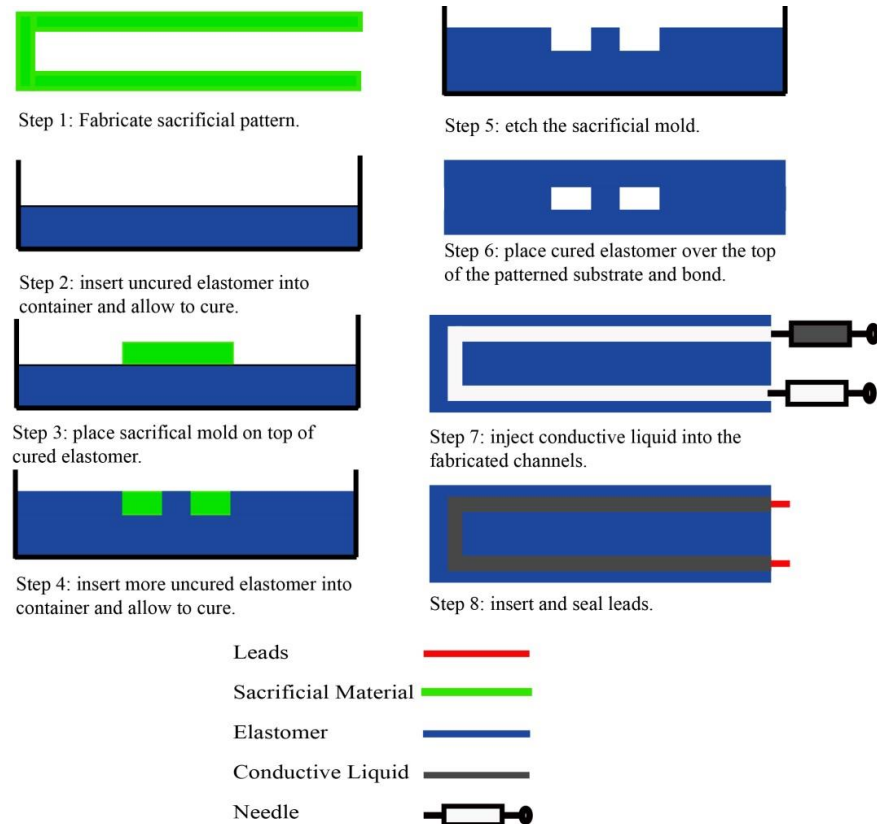


**Figure 2-1:** Representative diagram of molding process used to fabricate strain sensors

The molding process was implemented by Park *et al.* to fabricate a multi-axis strain sensor using Ecoflex as the elastomer, a 3D printed sacrificial mold, and eutectic Gallium Indium (eGaIn) as the conductive fill [6]. Park *et al.* created 3 layers to their strain sensor to measure strain in the XY directions and pressure in the Z direction. The fabricated strain sensor exhibited a GF of 3.6 and 3.7 for the x-axis and y-axis sensors,

respectively [6]. The dimensions of the channels used to hold the eGaIn in their strain sensor were 200  $\mu\text{m}$  wide and 300  $\mu\text{m}$  deep. Last, the maximum functional strain of the fabricated strain sensor was 250%. Other groups such as Lu *et al.* used a method where the channels were created layer by layer. First, channels were created by molding. Then the sacrificial channel section was etched. Then the carbon nanotube filler was input and the process repeated [8]. The strain sensor was fabricated using PDMS as the substrate and a Carbon Black doped PDMS as the conductive filler [8]. The strain sensor fabricated by Lu *et al.* was meant to operate at similar strains to human skin and was tested at strains levels 11% to 22% [8]. Lu *et al.* denoted a gauge factor as high as 29 for their strain sensor. Last, a design by Chossat *et al.* was also formed using the molding process [12]. The strain sensor used ecoflex as the elastomer and ionic liquids as the conductive filler. Upon creating the contacts to avoid the strain caused by typical wire electrodes a small nanocomposite structure was created to interphase the ionic strain sensing area with a eGaIn flexible contact area [12]. The maximum strain tested for the strain sensor was 100% and the GF was 3.08 [12].

### 2.3 Coating

The coating method involves introducing conductive properties to an elastic material by coating the elastic material in a conductive material [10]. The strain is measured based on changes in the conductivity or resistance of the material. In some cases, the coated material is encapsulated in a second layer of the elastic material in order to prevent it from being scraped off [7]. Additionally, in a few cases, the coating is absorbed into or bonded with the elastic material [10]. An example of the coating process is outlined in Figure 2-2.

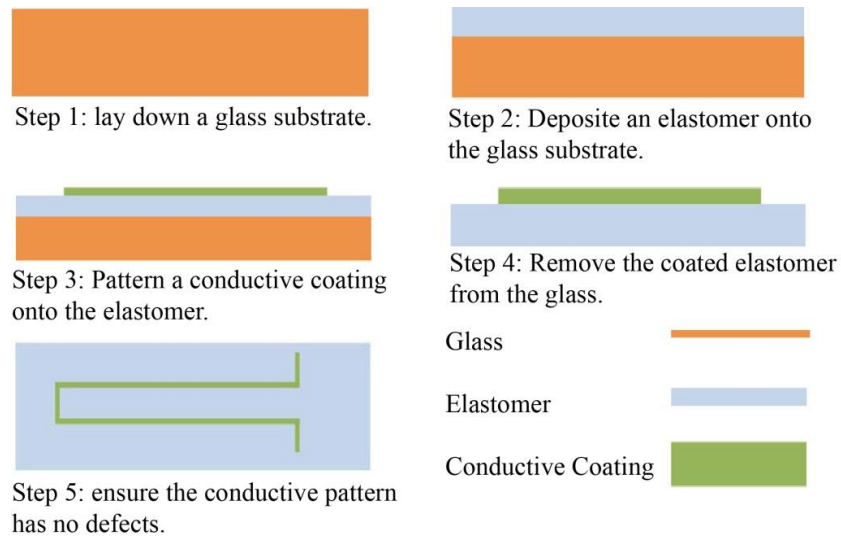


**Figure 2-2:** Representative diagram of coating process used to fabricate strain sensors.

Park *et al.* used a chemical process to implement nanowires or nanoparticles onto an electro-spun fiber weave [10]. Then a second chemical process further bonded the coating with the elastic substrate [10]. These strain sensors measure strain through changes in the conductivity based on the distribution of silver nanoparticles in the elastic substrate [10]. When the particles were near to each other, the conductivity was better as electrons could travel more easily from particle to particle [10]. As the object was stretched, fewer nanoparticles were in contact with each other thus causing a reduction in the conductivity [10]. Park *et al.* also found that the fibrous nature of their device caused stress accumulation and a strain offset to occur [10]. Stress accumulation was the buildup of stress in the fibers of the device. As the stress built up in the strain sensor, the fibers began to experience permanent deformation. This permanent deformation was what caused the strain offset. This finding indicated that the stress accumulation in the

individual fibers affected the conductivity of the entire strain sensor when recovering from higher strains [10]. Park *et al.* were able to achieve a maximum strain of 140% [10]. However, the device began to exhibit permanent deformations that altered the conductivity at strains greater than 40% [10]. A second example of coating was done by Lee *et al.* using silver nanoparticle thin films [4]. The process consisted of a silver nanoparticle thin film being directly deposited onto PDMS in a pattern. As the strain sensor was stretched microcracks formed in the thin film and, therefore, altered the conductivity [4]. The strain sensor was tested out to 25% strain with a GF of 2.05 at 20% [4].

## 2.4 Contact Printing

Contact printing is a method by which a patterned stamp is created. An example of contact printing is the shown in Figure 2-3.

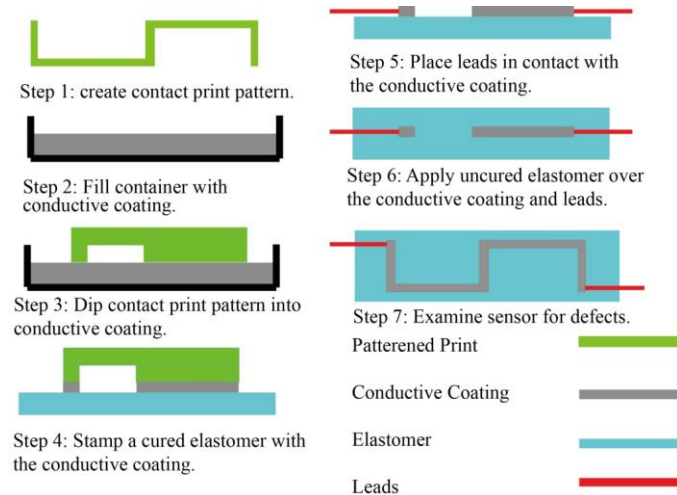


**Figure 2-3:** Representative diagram of the contact printing process used to fabricate strain sensors.

The Patterned stamp is dipped in a conductive material [11]. The conductive material is then deposited either on an elastomer or glass substrate [11], [13]. This is followed by an elastic material deposited over the substrate to encase the conductive stamp [13]. Liu *et al.* used the contact printing process to fabricate a strain sensor [11]. Liu *et al.* first fabricated a stamp through a printing process [11]. The stamp was then dipped in a PDMS nanocomposite that had been spin coated on to a plate [11]. From there the nanocomposite was then transferred to a glass surface in the shape of the stamp [11]. The pattern was then overlaid with PDMS. After the PDMS went through a curing process, it was then removed forming the flexible strain sensor [11]. The strain sensor was tested out to a strain of 41% and the GF was not reported. Another method of contact printing was used by Tabatabai *et al.* to form a flexible capacitive sensor [13]. Their method consisted of first spin coating a flexible silicon material onto a glass substrate [13]. Then using an open source 3D printer kit, the circuit was printed by first dipping a printer head into an eGaIn reservoir [13]. Then the eGaIn droplet was deposited onto the silicon [13]. The process was repeated until the desired pattern was formed. The terminals were then formed [13] and the capacitive strain sensor was frozen and coated with another layer of silicon to seal it [13]. The strain sensor was stretched 2.5mm and the capacitance change measured but the strain and the GF were not reported [13].

## 2.5 3D Printing

In 3D printing, the desired structure is manufactured by building up layers of elastic material. 3D printing is used in several ways to create strain sensors. In one way, 3D printing is used to fabricate molds or sacrificial layers in the molding process [1]. 3D printing can also be used to directly print strain sensors. A strain sensor was directly

printed by Muth *et al.* [2]. Muth *et al.* created a process called embedded 3D printing [2]. An example of the embedded 3D printing is shown in Figure 2-4:

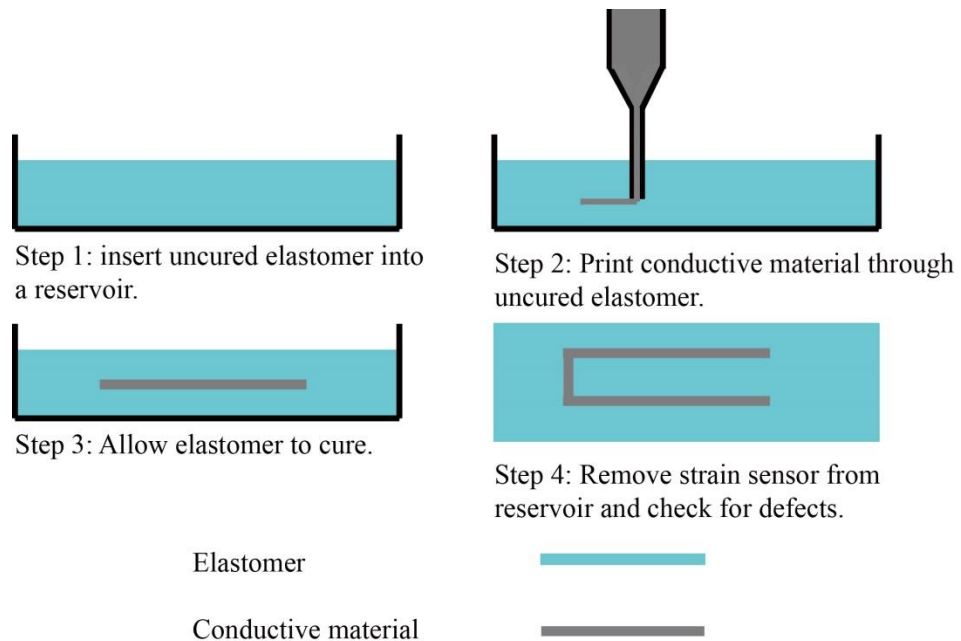


**Figure 2-4:** Representative Diagram of Embedded 3D printing based on Muth *et al.* procedure [2].

The process was designed specifically for printing flexible electronics by embedding a conductive ink into an elastomer. The process operates by having a reservoir filled with uncured elastomer and a filler fluid which covers the uncured elastomer [2]. The printer head injects the ink directly into the uncured elastomer in the designated pattern [2]. After the pattern was input, the elastomer was then allowed to cure, thereby, forming the strain sensor [2]. The strain sensor fabricated by Muth *et al.* had a gauge factor of 3.8 and a maximum effective strain of 400% [2]. One of the advantages of the strain sensor created by Muth *et al.* was that the strain sensor did not have the layers formed during the 3D print process. As a result, issues like layer

separation or adverse effects like strain offset, stress accumulation, or early permanent deformation were eliminated. However, Muth *et al.* noted that hysteresis still affected the results given by their strain sensor regardless of the lack of layering [2].

## **CHAPTER 3**

### **METHODS**

#### **3.1 Approach and Methods**

The experimental work was focused on fabrication, and characterization of the strain sensors. First, prototypes of the strain sensors were fabricated by 3D printing the strain sensors using Ninja flex Thermoplastic Polyurethane (TPU) flexible polymer. Two types of strain sensors were fabricated at different sizes to examine the effects of dimensions on the performance of the strain sensors, Type I with intended dimensions of 2000  $\mu\text{m}$  by 200  $\mu\text{m}$  and Type II with intended dimensions of 500  $\mu\text{m}$  by 200  $\mu\text{m}$ . Fabrication was then followed by characterization of the strain sensors. The performance of each type of strain sensor and their response to applied force was measured. Additionally, geometric fidelity and dimensional conformity of the fabricated strain sensors were examined to better understand their performance and limitations. Fabrication and characterization methods are described in this section.

#### **3.2 Approach**

Figure 3-1 shows the design of the strain sensors fabricated in this work. The strain sensors consisted of U-shaped embedded channels, conducting fluid, and substrate. The U-Shaped embedded channels consisted of long and short channels.

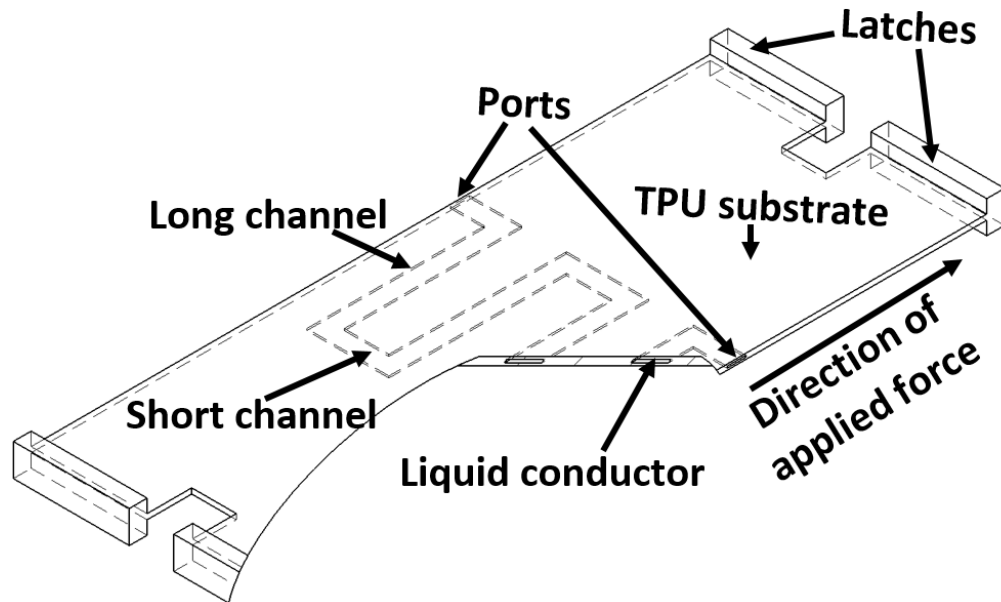


**Figure 3-1:** Cross-sectional view of the 3D printed strain sensor design.

When an external force was applied, the channels deformed and the cross-sectional area of the long channels reduced while the cross-sectional area of the short channels increased. As a result, the deformation of the long channels caused a reduction in the cross-sectional area of the conducting fluid. This change in area of the conducting fluid reduced the size of the path the current could flow through and thereby, increased its resistance. The conducting fluid used was Galinstan (Ga 68.5%, In 21.5%, Sn 10%) (Rotometals). Galinstan was chosen due to its good conductivity and low toxicity [14]. The pattern in the strain sensor was ideal for single axis strain. The main resistance change comes from the long channels that were parallel to the direction of the applied

strain. When strain is applied perpendicularly to the long channels, the resulting change in resistance was lower than when applied parallel. Figure 3-2 displays the operating principle of the strain sensor.

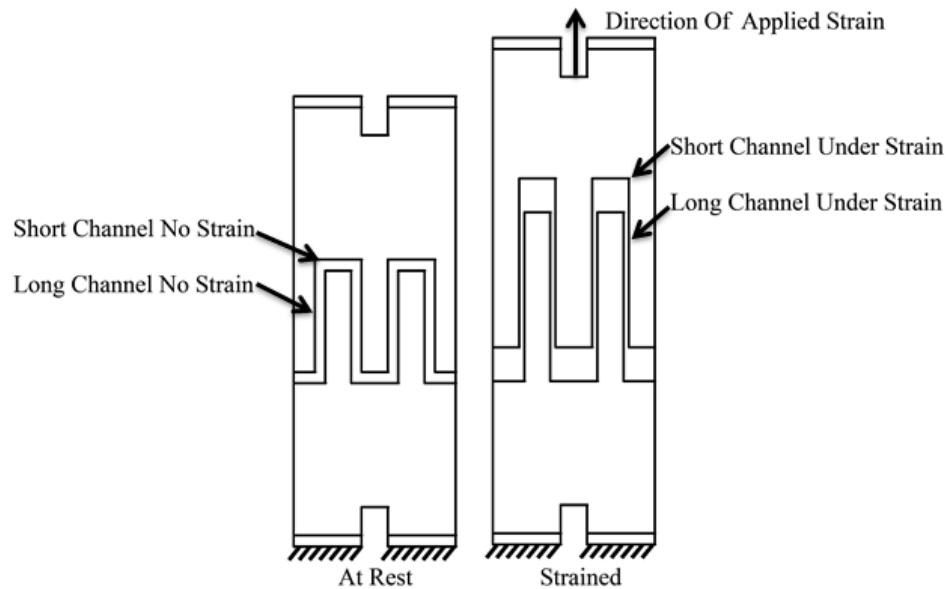


**Figure 3-2:** Working principle of the channel effects when under applied strained.

The strain sensor was set up such that the strain was parallel to the long channels. As shown in Figure 3-2, as the strain was applied the long channels surface area reduced while the short channels surface area expanded. Contraction was related to an increase in resistance while expansion caused a reduction in resistance. The contracting channels were made longer to prevent the gain in resistance from being balanced by the reduction in resistance. This leads to a single axis strain sensor.

### 3.3 Fabrication

The strain sensors were printed using a stock Ultimaker 3 FDM 3D printer. The material used to fabricate the strain sensors was Ninja Flex Thermoplastic Polyurethane

(TPU) shore hardness 85A (Ninjatek) and Poly Vinyl Acetate (PVA) (esun). Figure 3-3 shows dimensions and geometries of the strain sensors obtained using Solidworks software.

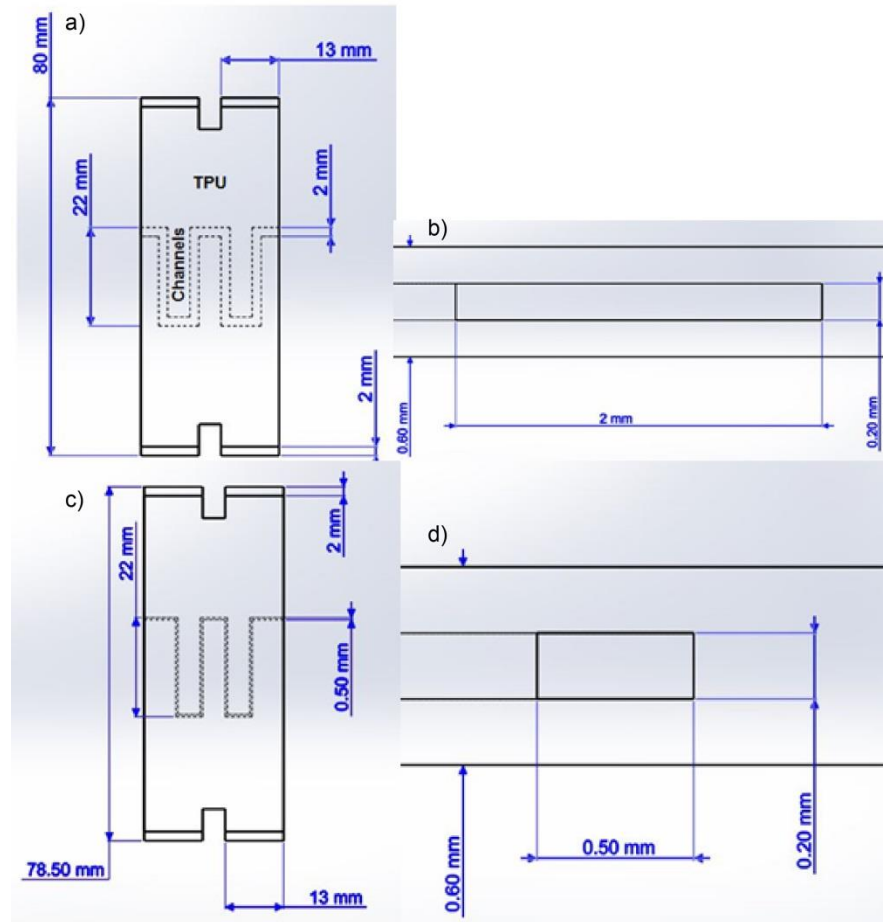


**Figure 3-3:** Design of strain sensor: a) Top view of Type I strain sensor and b) Side view of Type I channel port. c) Top view of Type II strain sensor and d) Side view of Type II channel port.

The first design Type I consisted of U-shape embedded channels with intended dimensions of width 2mm and height 0.2mm i.e. Figure 3-3(a-b). The second design Type II consisted of channels with intended dimensions of width .5mm and height .2mm, i.e. Figure 3-3 (c-d). The Type II sensors were fabricated with smaller dimensions to test

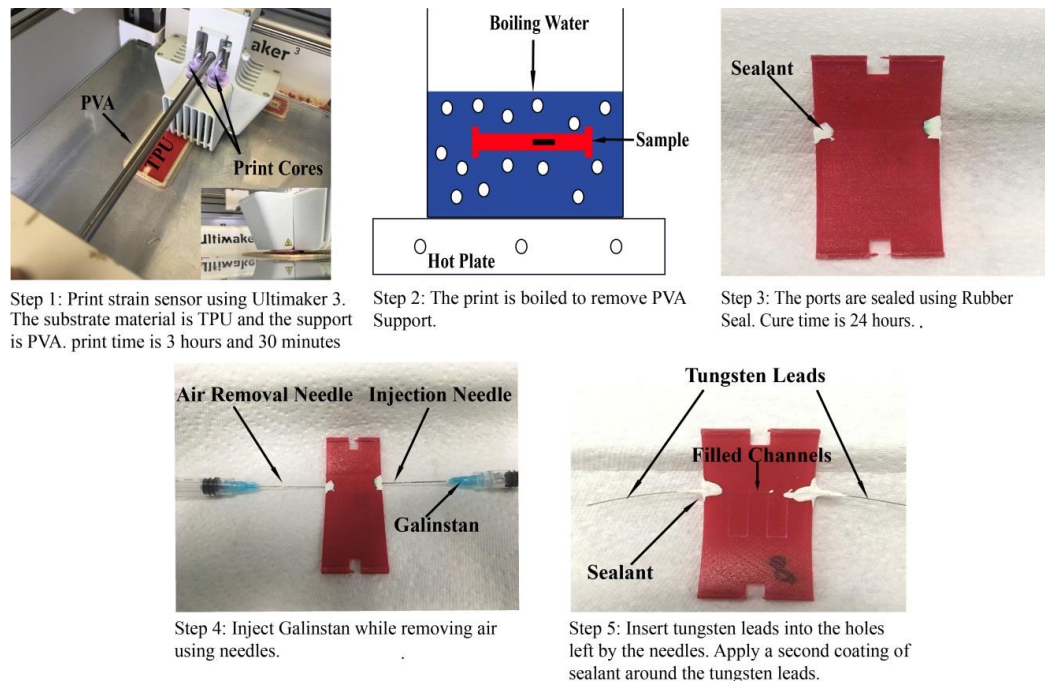
the limits of the printer as well as examine the effects of reduced channel dimensions on GF. Two ports were used to implement .016 gauge Tungsten leads (Malin Co.). The Tungsten leads were used to measure the response of the strain sensors. Tungsten was chosen as the material for the leads due to its high corrosion resistance since the Galinstan is highly corrosive towards other metals. Then the Solidworks file was saved as an .STL file which converted the file into a format compatible with the software Cura. Cura software is a slicer software used to set up the conditions of the print before sending it to the 3D printer. The setting and conditions used during the printing process are summarized in Table 3-1.

**Table 3-1:** Setting and parameters used to print the strain sensors using Ultimaker 3 FDM 3D printer.

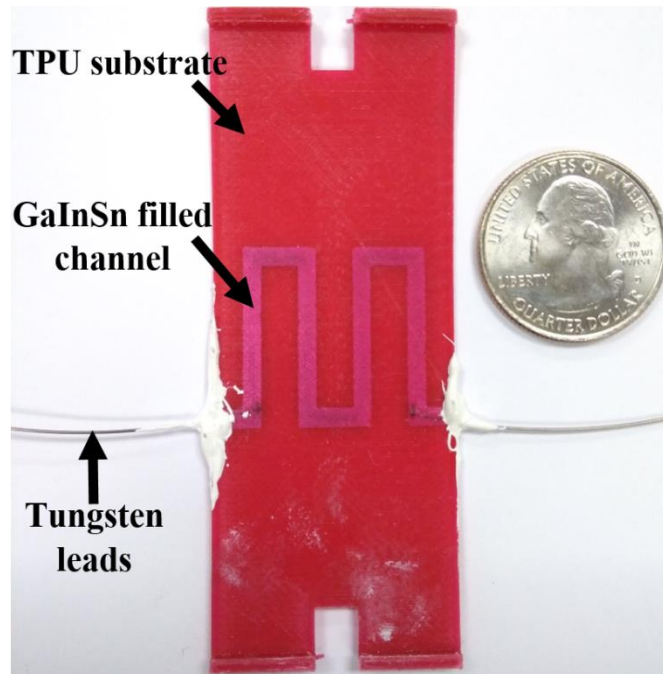
<b>Thermoplastic Polyurethane</b>	
Layer Height (mm)	0.04
Horizontal Expansion (mm)	0.16
Infill Density (%)	100
Infill Pattern	Grid
Printing Temperature (Degrees C)	245
Flow (%)	106
Speed (mm/s)	20
Generate Support	on
<b>Poly Vinyl Acetate</b>	
Layer Height (mm)	0.04
Horizontal Expansion (mm)	-0.16
Infill Density (%)	100
Infill Pattern	grid
Printing Temperature (Degrees C)	215
Speed (mm/s)	80

Figure 3-4 shows the fabrication process and assembly procedure of the strain sensors. The main structure of the strain sensors was made of Ninja Flex TPU while PVA was used as a support to prevent the channels from being filled in. Once the printing

process was completed the device was placed in boiling water for approximately 3-6 hours until the PVA was completely removed. The duration of the boiling process was determined by the support density and how well the support was printed. After clearing the support material from the channels Tungsten wires were carefully inserted into the ports of the strain sensors and sealed using liquid rubber (Rubber Seal). After curing for 24 hours, the liquid metal was injected through the cured seal. The injection process consisted of two needles one for injecting the Galinstan and the other for removing the air. The removal of the air and the injection of Galinstan were performed simultaneously. Sealant was reapplied to the strain sensor around the leads to ensure no leakage. The fully fabricated and assembled strain sensor is shown in Figure 3-5.



**Figure 3-4:** Representative diagram outlining the strain sensor fabrication process.



**Figure 3-5:** Fully fabricated and assembled strain sensor.

For the Type II channels, the process had to be modified slightly as the sizes of the inlet and outlet sections reduced significantly. This made it difficult to insert the needle through the glue for the injection process. Thus, the liquid metal was inserted before the sealing process was done. After the liquid metal was inserted, the leads were inserted and liquid rubber layered over top. The liquid rubber was then allowed to cure for 24 hours to seal the strain sensors.

### **3.4 Experimental Apparatus and Approach Towards Characterization of the Fabricated Strain Sensor**

Figure 3-6 shows the experimental apparatus used to characterize the fabricated strain sensors. The strain sensors were connected to a force gauge (Nidec Shimpo FG3006), laser displacement sensor (Keyence IL-100), multimeter (Fluke 87V) and a

circuit as shown in Figure 3-6. The circuit was used to measure the strain experienced by the strain sensors. This was done by running a constant 5V across a 120  $\Omega$  resistor that was connected in series with the strain sensors. A 120  $\Omega$  resistor was selected to increase the accuracy of the voltage change measurement, i.e. impedance matching. However, the resistance of the strain sensor was incredibly low and any resistor under 120  $\Omega$  began to heat up extensively. The voltage drop across the strain sensors was measured using a Fluke 87V multimeter. The strain sensors were first latched onto a pair of aluminum mounts that used threaded rods and wing nuts to hold the strain sensors. The strain sensors were then suspended from the force gauge by a hook and lowered until the bottom mount touched the stage as shown in Figure 3-6. After the strain sensors were lowered into place, the bottom mount was clamped to the stage. A pair of clips attached the strain sensors to the circuit. The multimeter was also attached to the tungsten leads to monitor the voltage drop. The strain sensors were then gradually strained from tension using the hand wheel on the test bench and readings were taken for the force, displacement and voltage as the values of the voltage drop changed steadily. Each test was performed 3 times per displacement value. After the test was performed, 3 times the displacement was increased by an increment of 5mm. Ohm's Law was used to estimate the approximate change in resistance,  $\Delta R$ , across the strain sensors that corresponded to the measured voltage drop. Strain,  $\epsilon$ , was calculated based on the length the strain sensor was stretched over,  $\Delta l$ , the original length of the strain sensor,  $l_o$ . From change in resistance,  $\Delta R$ , and strain,  $\epsilon = \frac{\Delta l}{l_o}$ , a strain-resistance curve was created. Similarly a,  $F$  vs  $\epsilon$  (force versus strain) curve was also made to examine how the force changed as strain was applied. GF calculations were performed on the data.

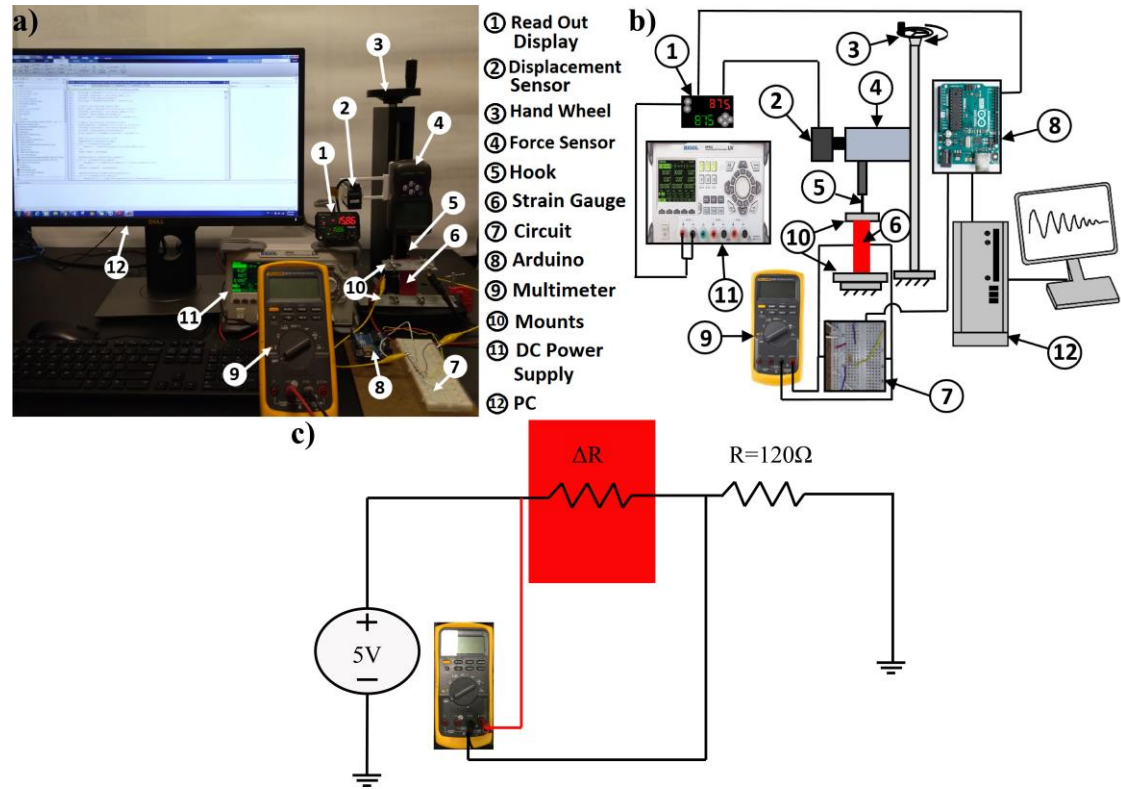


**Figure 3-6:** Experiment setup used for characterization of the fabricated strain sensor: a) Schematic diagram of experiment setup, b) Laboratory apparatus and c) circuitry diagram used for estimating voltage drop and resistance change.

### 3.5 Characterization of Channels

The 3D printed channels were characterized using a (VK-X100) confocal laser scanning (CLS) microscope. The CLS was used to examine channel dimensions and geometric fidelity. This was also done to document any oddities in the channel structure. Channels were printed without the top layer to allow for more accurate analysis of the channel dimensions across the strain sensor. The channels were then scanned using the CLS microscope. The VK analyzer software was then used to measure the cross section of the channel at multiple different points. The height of the channel was measured for each of the cross sections. The width was measured at the top, middle, and bottom of the

cross sections. In order to observe any variance in the channels, dimensions each channel type was printed and measured three times. All the measurements were exported and an average height and width were taken from the analyzed data. The average was then compared to the original Solidworks file and variance was determined. The fibers of the print were imaged to examine how the FDM process affected the elongation yield of the strain sensor. The corners of the Type II channels were imaged to examine the effects of bottlenecking on the strain sensor performance as will be discussed in Chapter 4 Section 4.2.

### **3.6 Tensile Test**

Tensile tests were used to examine the elongation of the strain sensor at yield. The strain sensors were tested using a Cell Scale tensile tester (Univert S/N 55144). Strain was applied cyclically to the strain sensor 3 times for each test. After the test the strain was increased by increments of 10%. The maximum measured strain the strain sensor was tested at was 71%. This was due to the size of the sample and the limitations of the tensile test machine. The data was taken from the tensile tester and the stress was calculated using the measured force. The stress was then plotted against the strain to form a stress-strain curve. The Young's modulus was also calculated. Figure 3-7 show the sample in the tensile test machine.

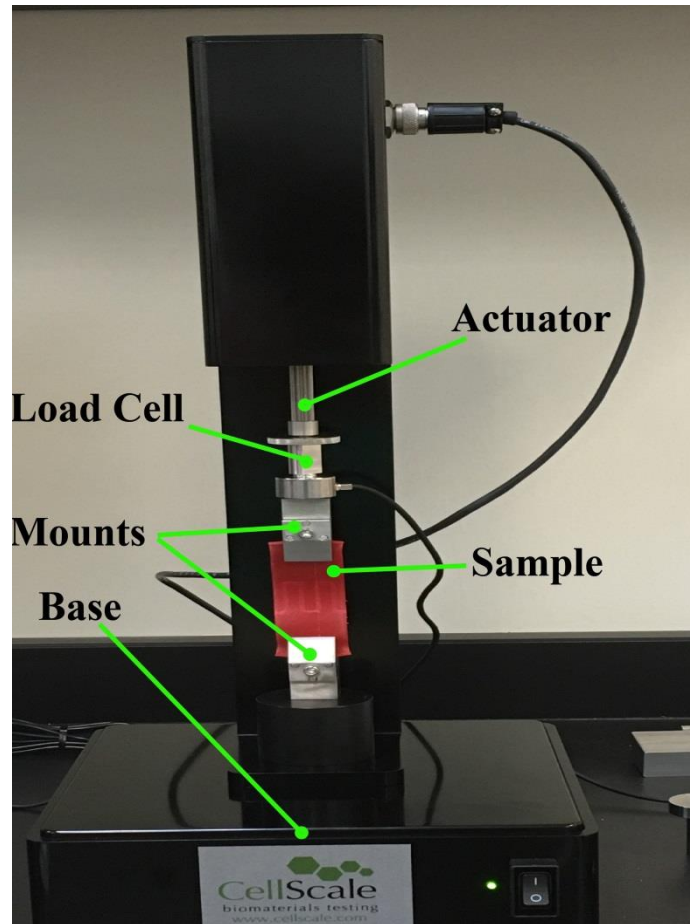


**Figure 3-7:** Tensile test setup with key parts labeled.

## **CHAPTER 4**

### **RESULTS**

#### **4.1 Results Overview**

The results of the strain sensor testing were divided into three sections. Section 4.2 is resistance vs strain and sensitivity testing. In this section, the strain sensors viability was tested by observing how well it measured strain. The sensitivity of the strain sensor was also examined in the form of the gauge factor. The strain sensors were modeled in COMSOL to examine the corner effects on smaller channels. Section 4.3 examines the force-displacement curves during testing and the tensile tests performed. The force-displacement curves were examined to observe the effects of strain on the substrate of the strain sensor. Further investigation was done by using a tensile test machine to observe the effects of stress on the substrate out to the manufacturer stated Young's modulus. COMSOL was also used to model and compare the stress distribution and strain of the strain sensors. From this, the effects of stress accumulation and strain offset were observed. Last, Section 4.4 examines the dimensional accuracy of the print. The channel dimensions are examined by taking the average dimensions of three samples and doing a variance analysis on them. Examining the print dimensions gives a better idea of how the accuracy of the printing process may affect the strain sensors performance.

## 4.2 Resistance VS Strain and Sensitivity Measurements

The strain sensor was fabricated with the objective of investigating the use of FDM 3D printing to form strain sensors. In this study the effectiveness of the strain sensor was verified by measuring change in resistance over initial resistance vs strain and gauge factor. The tests were performed using the test bench setup outlined in Section 3.4. The results of these tests were shown for both the Type I and Type II sensors.

Figures 4-1, 4-2, and 4-3 show the strain resistance curves for three Type I strain sensors referred to as Sample I, Sample II, and Sample III. For each test the samples were strained from tension and relaxed until tension was lost. The sensors were strained to 13.2%, 20.4%, 32.2%, 38.8%.

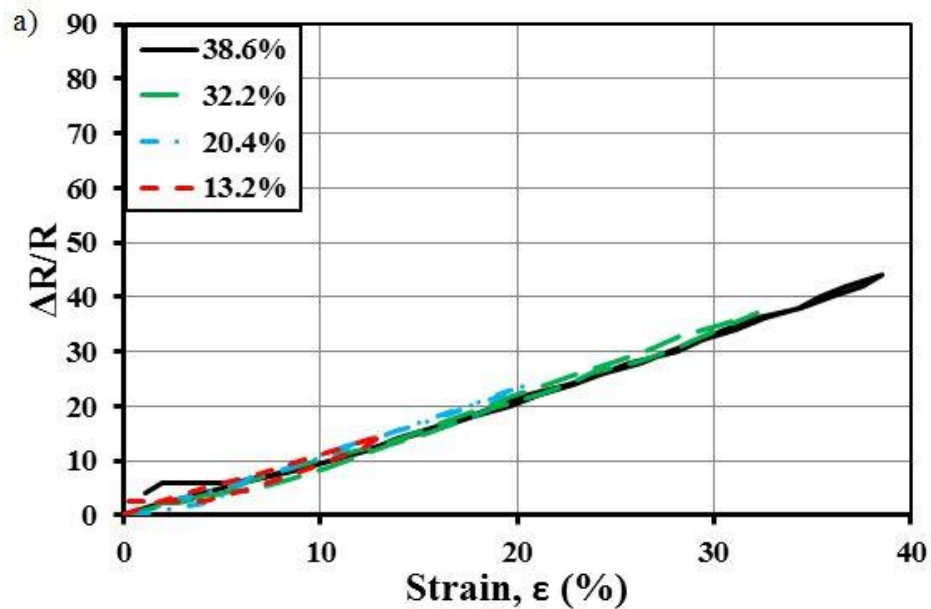


**Figure 4-1:** Resistance vs Strain Curve for Type I strain sensor Sample I.

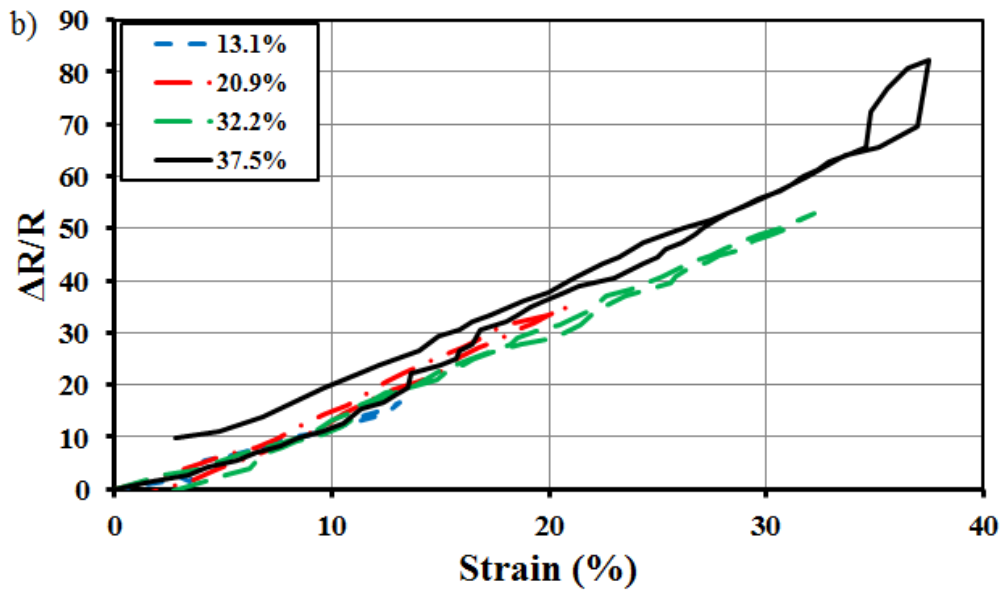


Figure 4-2: Resistance vs Strain Curve for Type I strain sensor Sample II.

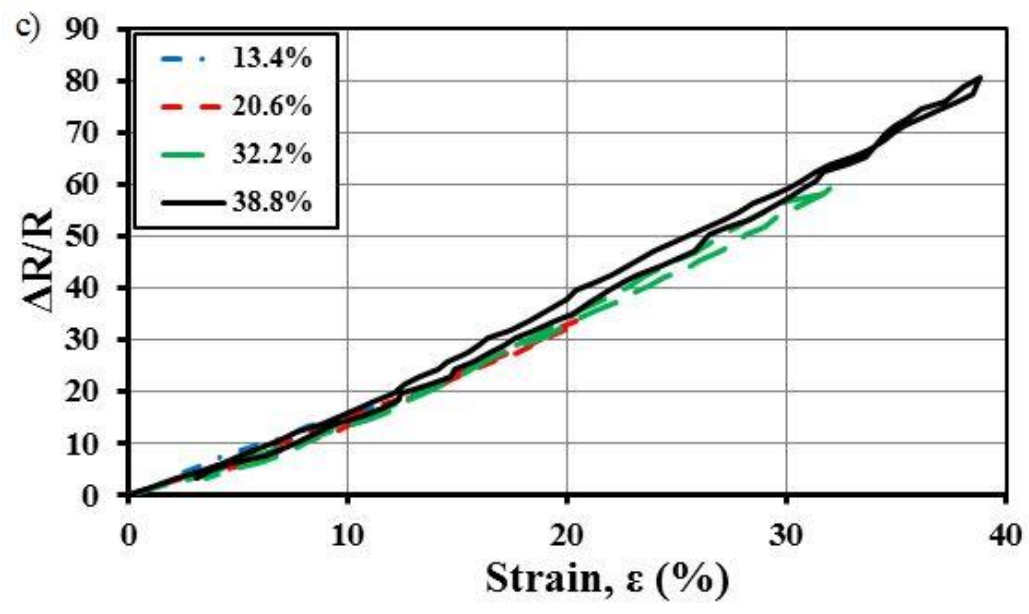


Figure 4-3: Resistance vs Strain Curve for Type I strain sensors Sample III

The results of the tests on Samples I, II and III showed a linear relation for the range of strains tested. The results also showed relatively little hysteresis for strains

higher than 13.2% for Sample I. This can be determined from the relatively small area under the curve for strains higher than 13.2% for Sample I. For Sample II the results still show a linear trend. However, the hysteresis was slightly worse than Sample I for 37.5% strain. Sample III showed little to no hysteresis overall. The sensitivity of the strain sensors was determined from the calculated gauge factor. The gauge factors of the strain sensors are shown in Table 4-1 along with their initial length and starting resistance.

**Table 4-1:** Strain, initial length, initial resistance, and calculated gauge factors for the three strain sensor samples.

Sample I		Sample II		Sample III	
Strain (%)	GF	Strain (%)	GF	Strain (%)	GF
13.20%	1.1	13.10%	1.3	13.40%	1.5
20.40%	1.2	20.80%	1.7	20.60%	1.7
32.20%	1.2	32.20%	1.6	32.20%	1.9
38.60%	1.1	37.50%	2.2	38.80%	2.1
$L_0$	$R_0$	$L_0$	$R_0$	$L_0$	$R_0$
79.14	98.4	81.17	173.0	79.03	129.7

GF was affected by multiple different aspects of both resistance and strain. Firstly there was the relationship between initial resistance and change in resistance. Throughout testing changes in the initial resistance were noticed as the strain sensor was strained more. This change in initial resistance was caused by stress accumulation. As the strain sensor was strained, stress accumulated in the TPU substrate. The accumulated stress caused the channels to deform as the substrate was relaxed from higher strains. The change in the channels' initial dimensions was related to the rise in initial resistance. The rate at which the resistance changed was approximately linear. The ratio between initial resistance and change in resistance changed between increases in applied strain. This

caused the change in GF. Also of note was the initial length as initial length was used to determine the displacement required to achieve a certain strain percentage. Thus, the slight variation in size of the strain sensor would make a difference in how much the strain sensor was displaced. Although this does not make any difference to a single sensor, it would partially account for differences in GF between strain sensors alongside overall channel dimensions and fabrication quality.

The effect of stress accumulation is further examined in Figure 4-4. Figure 4-4 shows the accumulation of stress in the TPU substrate and the effects of the accumulated stress on the initial resistance.

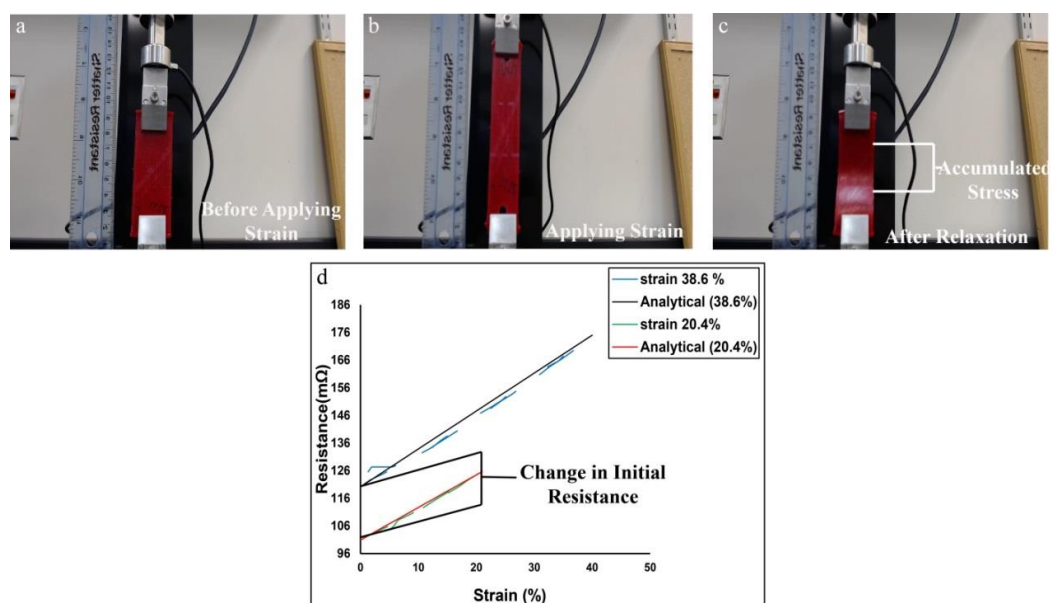


**Figure 4-4:** Tensile test process and a chart of resistance vs strain to demonstrate the effect of stress accumulation. a) Strain sensor substrate before strain b) Strain sensor substrate during strain c) Deformed strain sensor substrate due to stress accumulation d) Effect of stress accumulation on initial resistance.

Figure 4-4a-c shows the TPU substrate before during and after a high strain tensile testing. The stress accumulation can be seen in Figure 4-4c from the bend in the substrate during relaxation. The bend in the substrate was due to the accumulated stress in the fibers of the substrate. Similarly, the effect of accumulated stress on initial resistance can be seen in Figure 4-4d. There was a significant change in resistance between 20.4% and 38.6% strain. The rise in initial resistance due to accumulated stress was important as initial resistance affected GF. Also of note is the difference in the GFs between Sample I and Samples II and III. Samples II and III had higher GFs meaning they had better sensitivity than Sample I. The reason behind this was the difference in the starting resistances as well as the change in resistance per unit strain of the devices. Although Samples II and III had higher starting resistances than Sample I, their change in resistance per unit of strain was also higher. This led to Samples II and III having better GFs than Sample I as the ratio of  $\Delta R$  to  $R$  was better for Samples II and III.

The channel dimensions were reduced to .5 mm by .2 mm for the Type II strain sensors to test the effectiveness of the FDM process at small scale. The reduction in dimensions caused an increase in the change in resistance for similar strain application. However, the reduction in channel dimensions also increased the initial resistance. Thus the Gauge factor was slightly lower than that of the Type I samples. Figure 4-5 shows the change in resistance over initial resistance vs. strain for the smaller channels.

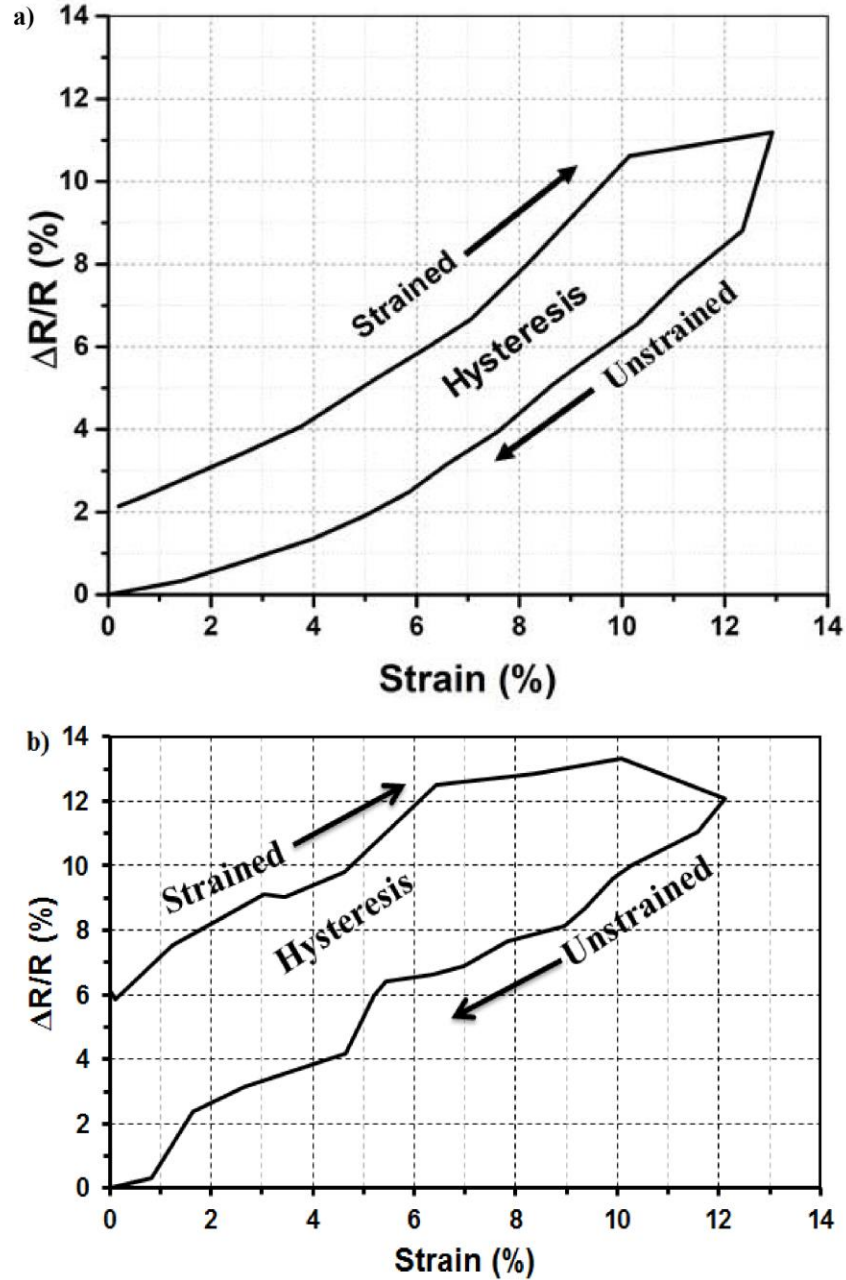


**Figure 4-5:** Change in resistance vs. strain for the Type II strain sensor. a) Sample IV b) Sample V.

The change in resistance of the Type II strain sensors was significantly higher at lower strains than the Type I strain sensors. At 13% the Type II samples had a  $\Delta R$  of 246 m $\Omega$  and 266 m $\Omega$  for Sample IV and Sample V respectively. The Type I samples had a

$\Delta R$  of 14.4 m $\Omega$  for Sample I, 16.7 m $\Omega$  for Sample II and 20.4 for Sample III. However, the drawback of the reduced channel dimensions was an increase in hysteresis, initial resistance, and reduction in maximum strain. The initial resistance of the Type II strain sensors was 2207 m $\Omega$  and 2212 m $\Omega$  for Sample IV and V respectively. The GF of the Type II samples was .866 for Sample IV and .996 for Sample V. The GF is due to the ratio of  $\Delta R$  to  $R_0$ . The increased change in resistance was offset by the increase in initial resistance. Thus, although the channel dimensions are smaller the sensitivity was still lower than Samples I, II, and III. The Type II strain sensors failed above 13% strain giving them a lower max strain than the Type I strain sensors. The Type II strain sensors failed due to continuous increases in resistance during relaxation. The increases in resistance were likely due to defects at the corners of the channels that were observed experimentally.

The corners of the channels were imaged to better understand the increase in resistance. The corners of the channels showed bottlenecking. Bottlenecking occurred when the channel had a significant reduction in width. When stress was applied past 13% the corner began to pinch. These corner effects were imaged using the VK X-100 CLS microscope and stresses around the corner modeled using COMSOL. Figure 4-6 shows the microscope images as well as the modeled stresses.

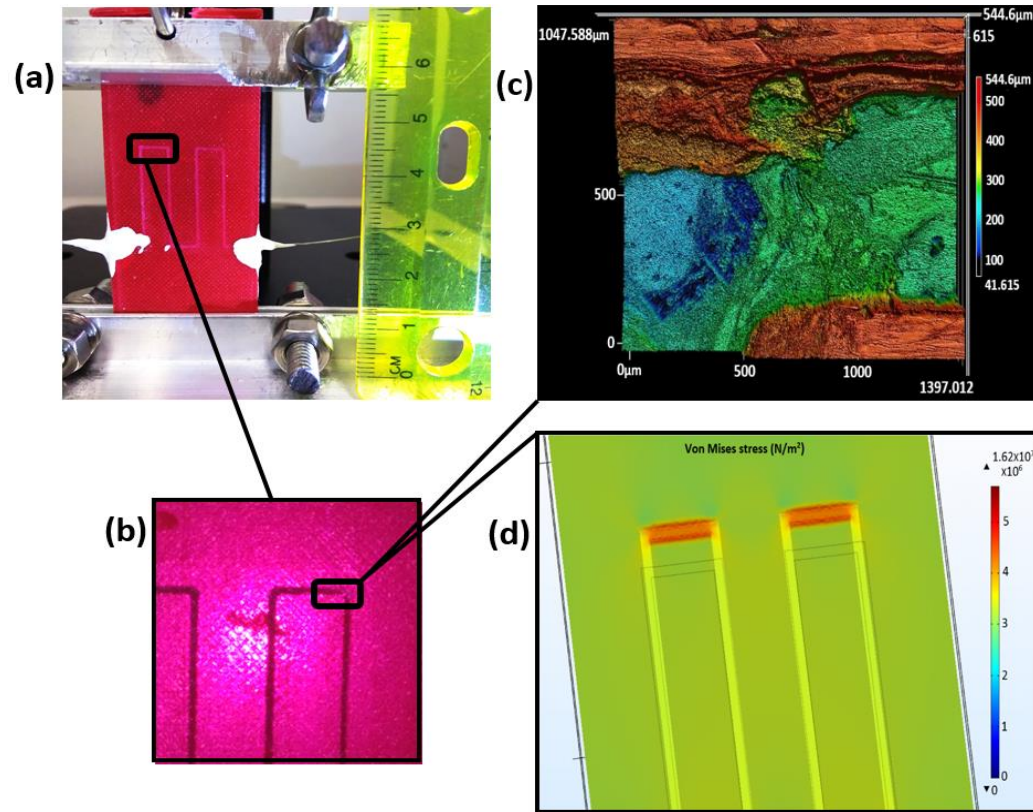


**Figure 4-6:** Failure of Type II strain sensors a) strain sensor in testing setup under tension b) image of bottleneck that exists at the corner. c) CLS 3D image of the bottleneck observed during dimensional characterization. d) COMSOL model of stress concentrations near the corners.

The corner effect seen in Figure 4-6 was a bottleneck defect formed during the printing process. The bottlenecks caused large reductions in the channel dimensions and occurred frequently at corners. Figure 4-6c shows a 3D scan of a corner bottleneck and a reduction in channel dimension. Figure 4-6d shows a model of the stresses on the corners during strain application. The combination of the bottleneck, high-stress concentration, and stress accumulation caused pinching in the corner. This pinching caused the Galinstan to separate around the corner as can be seen in Figure 4-6b. Galinstan has a high surface tension thus after it separated around the corners it did not return to its original form during strain relaxation. Thus this separation caused a significant increase

in resistance R. This significant increase in resistance R resulted in the failure of the Type II samples above 13% strain.

### 4.3 Force Displacement and Tensile Tests

During the resistance strain tests the force on the strain sensor was also taken. The force was plotted against displacement to examine how it changed during the test. Tensile tests were also performed to examine the Young's modulus and the effects of stress accumulation on the substrate. First, the force-displacement curve for a Type I sensor is shown in Figure 4-7.

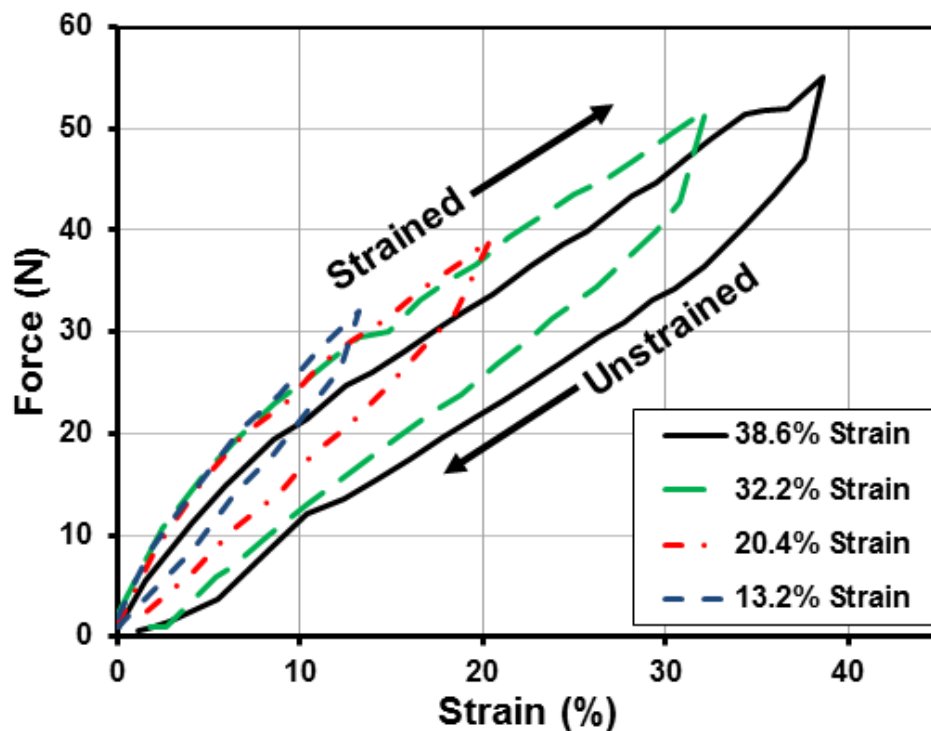


**Figure 4-7:** Force-displacement curve of Type I strain Sensor out to the maximum tested strain.

Figure 4-7 suggests that lower strains have lower hysteresis based on the smaller area under the curve. There was a significant difference between the 38.6% strain and

32.2% strain curves. At 38.6% strain lower forces were observed compared to 32.2%. The lower forces at 38.6% are due to relaxation of the TPU fibers. To better examine the effects of relaxation cyclic strain and unstrained tests at 32.2% were performed and shown in Figure 4-8.

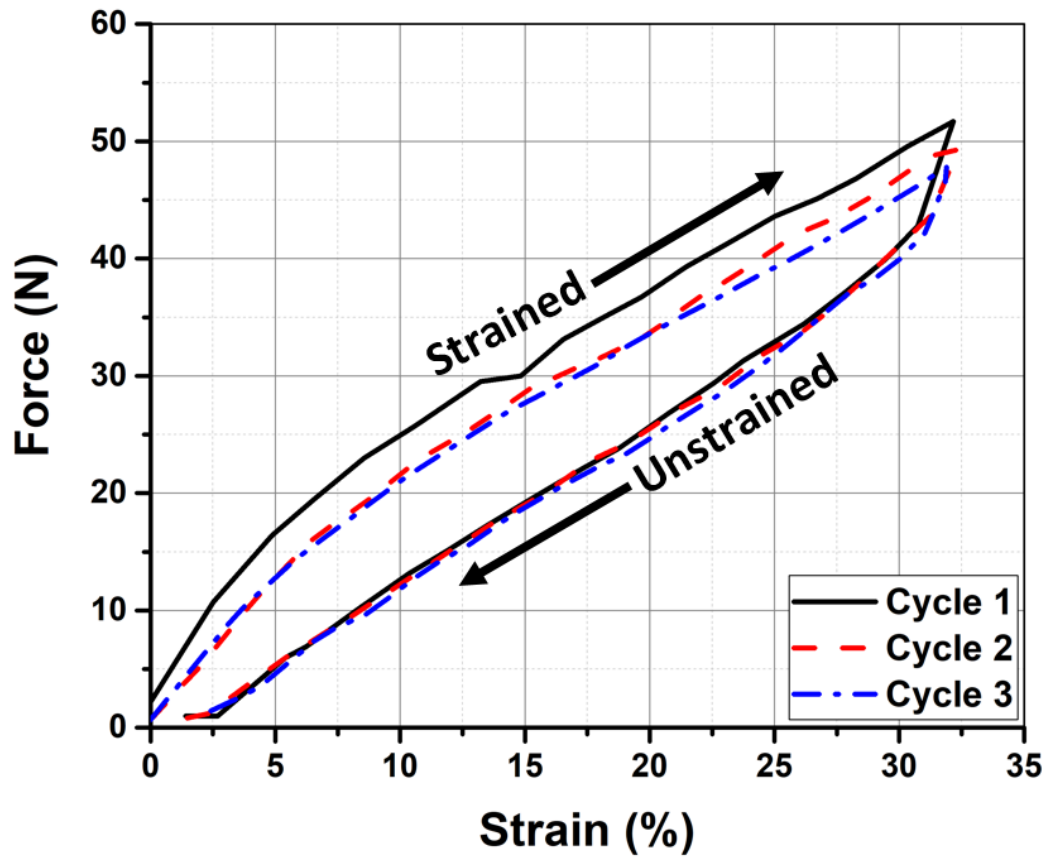


**Figure 4-8:** Relaxation effects as a result of cyclic straining/unstraining of the 3D printed sensor substrate.

Figure 4-8 shows that after the first cycle at 32.2% strain the fibers of the strain sensor relaxed causing the amount of applied force during the second cycle to be lower. The data in Figure 4-9 shows that with each cycle the force relaxed until at the 3<sup>rd</sup> cycle at 32.2% matched the first cycle of 38.6% strain.

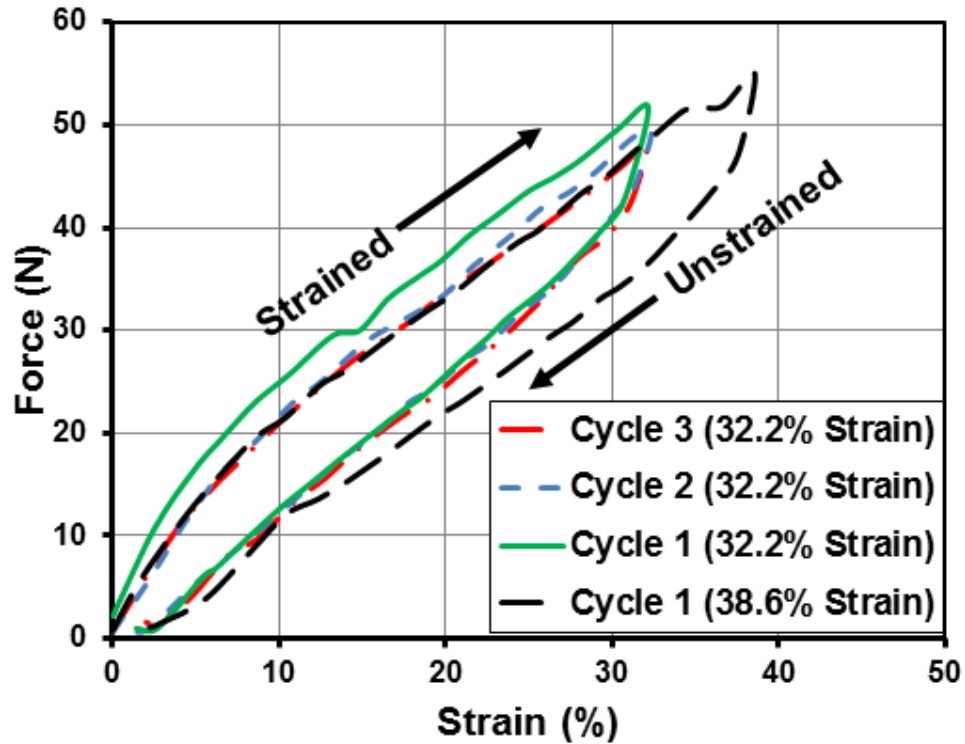


**Figure 4-9:** Comparison of 32.2% Force vs Strain after 3 cycles to 38.6% Force vs Strain.

The effects demonstrated in Figures 4-7, 4-8, and 4-9 were similar to ones noted by Park *et al.* [10]. With each cycle, the fibers relaxed causing the next cycle to be lower. This strain offset was due to the stress accumulation and fiber direction in relation to applied strain.

Strain offset and stress accumulation were relevant to the FDM printing process as structures were printed line by line. Figure 4-10 shows an image of the fiber-like nature of the FDM print.

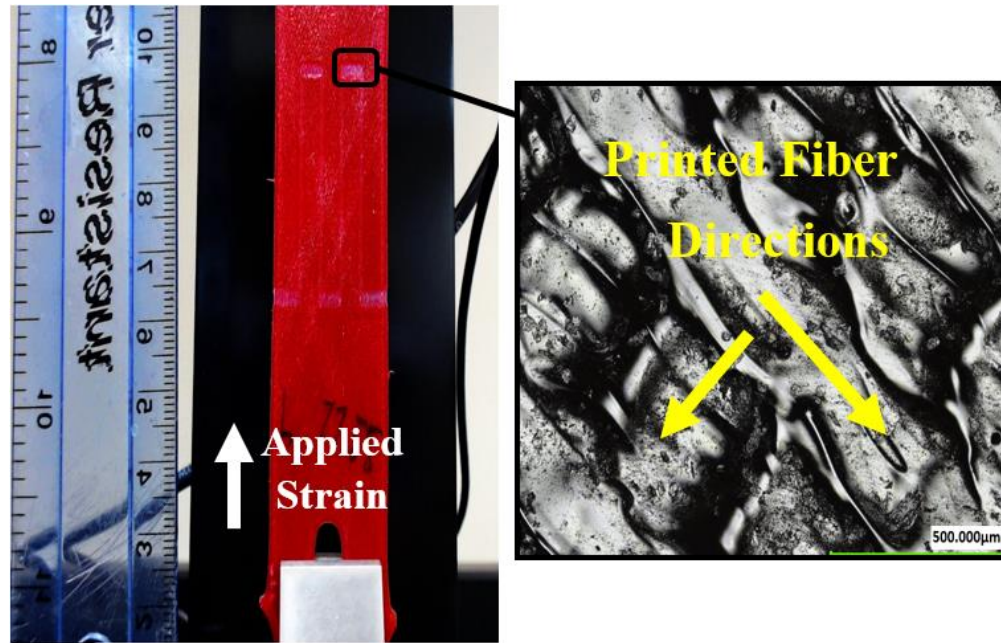


**Figure 4-10:** Image of strain sensor with zoomed in image of filament fibers shown in diagonal crossing pattern with respect to applied strain.

In Figure 4-10, the direction of the filament fibers was diagonal across the strain sensor and perpendicular to each other. The applied strain was at a 45-degree angle to the fiber direction. Thus, the strain offset and permanent deformation were partially caused by the angle of the applied strain. Since the force was applied at an angle to the fibers printed direction, the strain was applied to the width of the fiber rather than the length. The width being significantly shorter than the length yielded faster. Thus, the strain sensor experienced permanent deformation and stress accumulation faster than if the fibers were aligned with the strain. The way the FDM process formed the TPU substrates was such that the fibers were usually at an angle to the applied strain. This reduced the strain required to cause an accumulation of stress in the fibers. These observations were highly relevant to the creation of 3D printed strain sensors as the patterning of the layers can alter the strain response of the strain sensor significantly.

Tensile tests were performed on the strain sensor to better examine the effects of strain on the TPU substrate. Figure 4-11 shows the results of the tensile test for the Type I strain sensor.

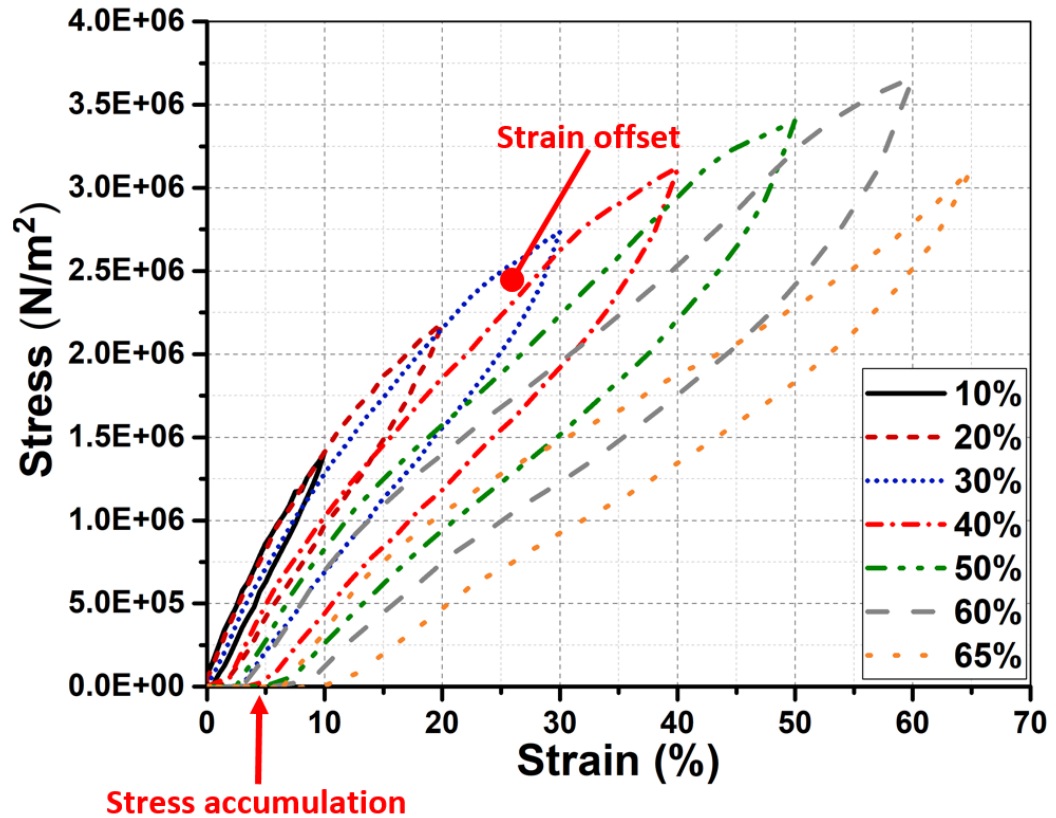


**Figure 4-11:** Stress-strain curves obtained from tensile tests showing strain offset and stress accumulation experienced by the 3D printed samples.

In Figure 4-11 the strain offset occurred around 30% to 40% strain. The tensile yield point of the strain sensor was 65% strain. The effects of the stress accumulation can also be seen in the lower left corner of the stress-strain curves. After 30% strain, the strain sensor did not return to its original length. This effect only increased as the strain sensor was strained more since the stress accumulates more with each cycle. The stress accumulation in the strain sensor affects the channel dimensions. Once the strain sensor

was relaxed, the channel dimensions did not necessarily return to their original length at higher strain. This caused a change in the initial resistance across the strain sensor. The Young's modulus found through tensile testing was approximately the same as the Young's modulus reported by the manufacturer.

#### **4.4 Geometric Fidelity of Strain Sensor Channels**

The dimensions of the channels for both the Type I strain sensor and the Type II strain sensor were examined. Three samples were examined for both the Type I and the Type II channel dimensions. The channels were imaged in their entirety using the VK X100 CLS microscope. The imaging process split the entirety of the channel into image segments. Within each image segment, three height measurements and nine width measurements were taken for the Type II channels. For the Type I channels, the image segments had to be compiled into a single large image to be measured. This was due to the width of the Type I channels exceeding the maximum image segment dimensions. After imaging 8 height measurements and 24 width measurements for the short channels and 10 height measurements and 30 width measurements for the long channels. Figure 4-12 shows an example of the measurement process.

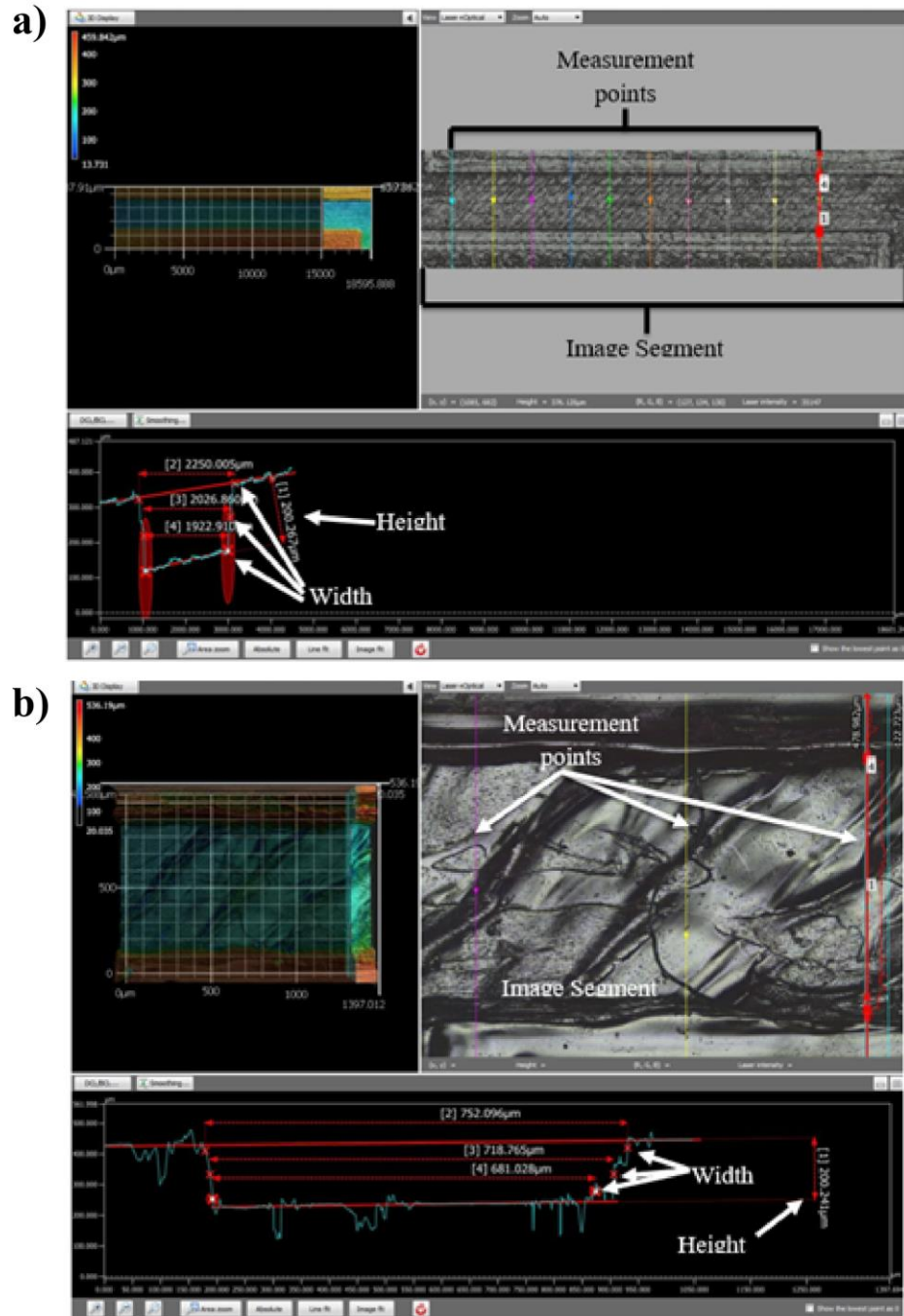


**Figure 4-12:** Images of the analyzer software as it was used to measure dimensions. a) Image of Type I channel measurement process. b) Image of Type II channel measurement process.

The measurements taken using the process outlined in Figure 4-12 were exported to excel. Then an average of all width and height values across the three samples was taken. The average channel width and height across the three samples was then plotted and a variance calculation was done. Table 4-2 shows the Solidworks dimensions as well as the actual measured dimensions of height and width for the Type I and Type II strain sensors.

**Table 4-2:** Measured dimensions of 3D printed sensors

Sensor Design	Intended Width X Height ( $\mu\text{m}$ )	Measured width ( $\mu\text{m}$ )	Measured height ( $\mu\text{m}$ )
Type I	2000 X 200	2100.56 $\pm$ 60.78	198.99 $\pm$ 14.12
Type II	500 X 200	696.47 $\pm$ 73.40	203.33 $\pm$ 5.06

Table 4-2 shows the average width of both the Type I and the Type II strain sensors as well as the intended width. The average width dimensions were higher than intended. Rather than being around 2000  $\mu\text{m}$  or 500  $\mu\text{m}$  they were closer to 2100  $\mu\text{m}$  and 690  $\mu\text{m}$ . The average width had a variation of 60  $\mu\text{m}$  and 73 $\mu\text{m}$  for the Type I and the Type II strain sensors, respectively. However, the height of the channels for both the Type I and the Type II sensors had good dimensional fidelity. The variance of the height was 14  $\mu\text{m}$  and 5  $\mu\text{m}$  for the Type I and Type II strain sensors, respectively. The discrepancy in the dimensional fidelity was due in part to the capabilities of the printer and the print settings. The accuracy of the printer was lower in the XY direction than in the Z direction. Thus more variance occurred in the width of the channels than in the

height. However, the reason for the significantly larger average dimensions was due to the use of horizontal expansion. Horizontal expansion was used to offset thermal expansion of the plastic during the printing process.

The 3D printed sensors presented in this work were also compared with state-of-the-art resistive strain sensors shown in Table 4-3.

**Table 4-3:** Comparison of recently reported resistive flexible strain sensors selected from the literature.

Author(s)	Fabrication	Gauge Factor	Strain level
This work	Additive manufacturing	1-2	38.6%
Muth et al.[2]	Embedding a conductive ink into an elastomer	3.8	400%
Park et al.[6]	Layered molding and casting of channels in an elastomer matrix filled with conductive liquid	3.93	250%
Amjadi et al.[7]	Carbon nanotube thin film on Ecoflex layer	2.5	500%
Yamada et al. [15]	Carbon nanotube thin film on PDMS substrate	0.82	280%
Kang et al. [9]	Depositing platinum layer on top of a viscoelastic polymer	2000	2%
Agarwala et al.[16]	Inkjet printing using photopolymer composite material	50	1%
Kong et al. [17]	micropatterning of conductive composites on PDMS	5.5	10%

Although the 3D printed sensors reported in this work were not optimized their performance compared well with other resistive-type strain sensors fabricated using other technologies. Table 4-3 demonstrates the potential of additive manufacturing to compete against other advanced and complex techniques to produce complex designs and a variety of small-scale devices that can be utilized in a wide range of applications. Unlike other representative techniques reported in Table 4-3 [4, 11, 16-20] the use of 3D printing to directly create the sensor structure is rather simple and straightforward. The simplicity of fabrication and the ability to adopt complex designs make additive manufacturing an attractive method for realization of these sensors. It is noteworthy to mention that this work is focused on initial designs and proof-of-concept attempts rather than optimization of the proposed design. Several improvements can be made to enhance the performance and GF metrics of the 3D printed strain sensor.

## CHAPTER 5

### CONCLUSIONS AND FUTURE WORK

#### 5.1 Conclusions

Flexible single-axis strain sensors have been fabricated using commercially available elastic filaments and desktop Fused Deposition Modeling (FDM) 3D printer. The viability of the strain sensor has been analyzed by relating changes in resistance to changes in strain, i.e., gauge factor. Two sensor configurations have been adopted. Type I strain sensors were fabricated and measured, gauge factors within the range of 1 to 2 were observed at approximately 38.6% strain with high linearity and low hysteresis. Moreover, Type II strain sensors were fabricated measuring  $696\ \mu\text{m}$  by  $203\ \mu\text{m}$ . The Type II strain sensors had measured gauge factors of approximately 0.9 at 13% strain. The potential for producing complex designs and a variety of sensor platforms using desktop FDM printing technique has been demonstrated. Nonetheless, issues related to strain offset, stress accumulation, and stress concentration were limiting factors. The way the FDM process formed the elastic substrates was such that the fibers were interwoven and at an angle with respect to the applied strain. This reduced the strain required to cause permanent deformation and strain accumulation in these fibers. These observations were highly relevant to the creation of 3D printed strain sensors as the patterning of the layers could alter the strain response of the strain sensor. Overall, FDM 3D printing has

been shown to have potential as a method of simple and cost-effective fabrication of flexible strain sensors.

## **5.2 Future Work**

Future work should focus on investigating the effect of printing settings such as horizontal expansion, speed, and temperature on bottlenecking at channel corners. Reducing stress concentration by implementing rounded shapes and avoiding sharp edges might also improve the maximum strain levels of the sensor. Last, exploring other rubber-like materials may also improve the metrics of the sensor.

## APPENDIX A

## RAW DATA FOR RESISTANCE VS STRAIN CHARTS

## A.1 Type I Strain Sensor

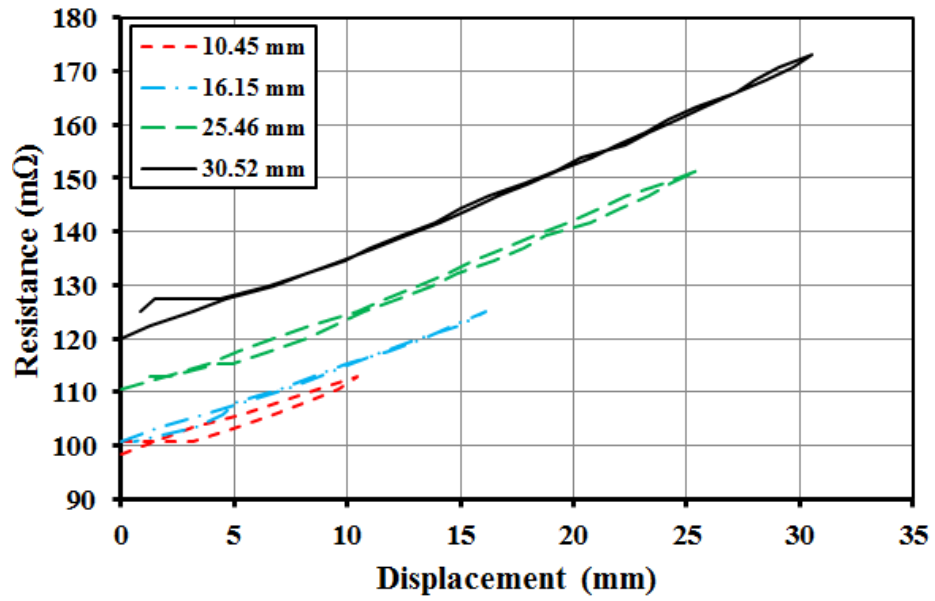


Figure A-5-1: Resistance vs Displacement curve Sample I.

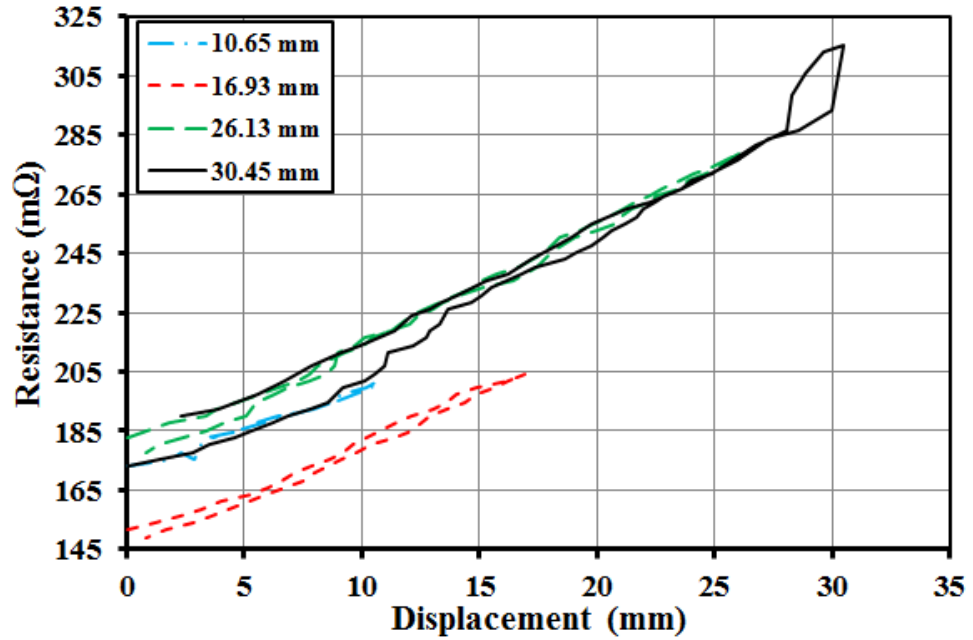


Figure A-5-2: Resistance vs Displacement curve for Sample II.

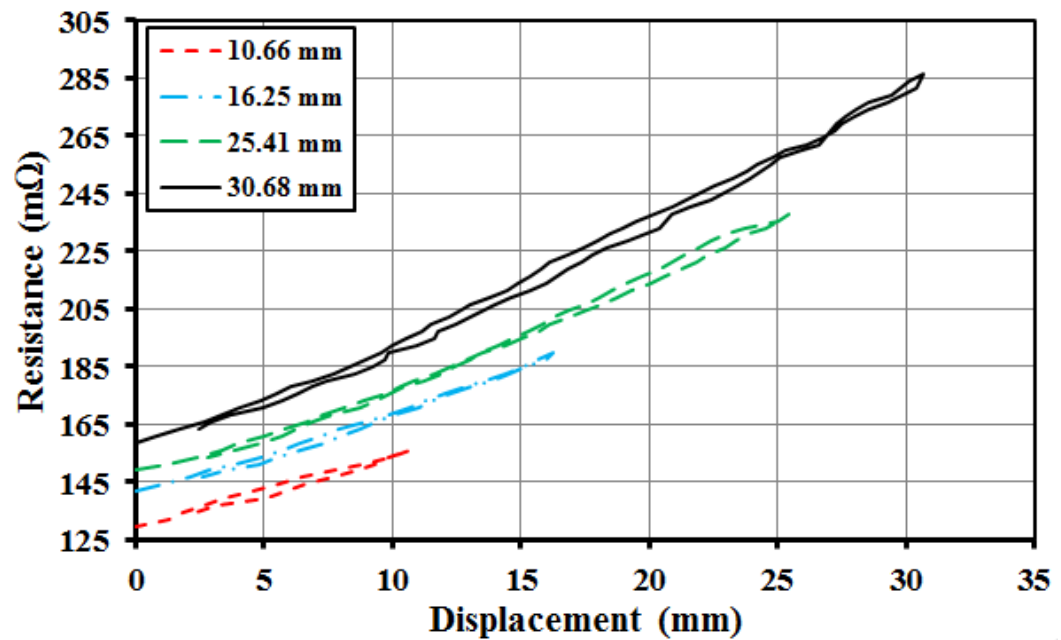


Figure A-5-3: Resistance vs Displacement curve for Sample III.

## A.2 Type II Strain Sensor

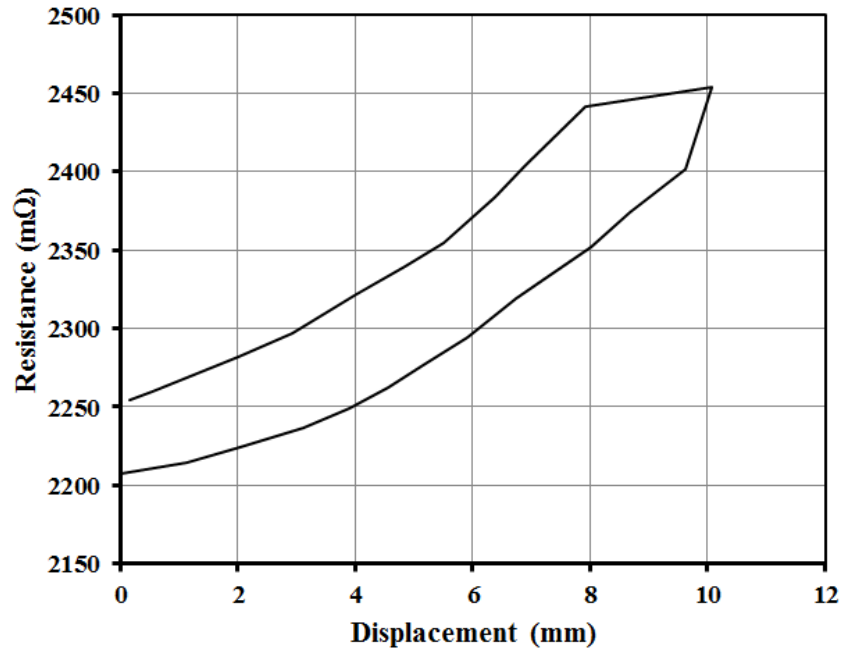


Figure A-5-4: Resistance vs Displacement curve for Sample IV.

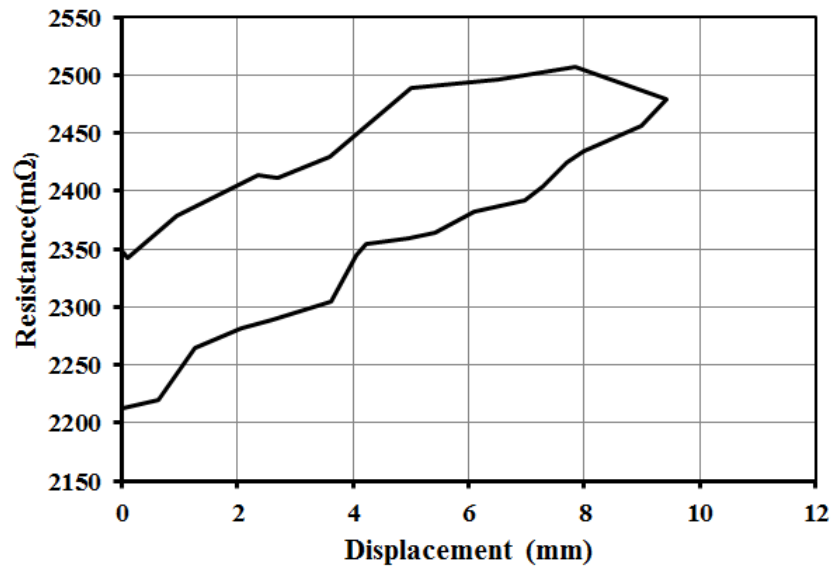


Figure A-5-5: Resistance vs Displacement curve for Sample V.

## BIBLIOGRAPHY

- [1] M. Amjadi, K. U. Kyung, I. Park, and M. Sitti, “Stretchable, Skin-Mountable, and Wearable Strain Sensors and Their Potential Applications: A Review,” *Adv. Funct. Mater.*, vol. 26, no. 11, pp. 1678–1698, 2016.
- [2] J. T. Muth, D. M. Vogt, R. L. Truby, Y. Mengüç, D. B. Kolesky, R. J. Wood, and J. A. Lewis, “Embedded 3D printing of strain sensors within highly stretchable elastomers,” *Adv. Mater.*, vol. 26, no. 36, pp. 6307–6312, 2014.
- [3] D. Vogt, Y.-L. Park, and R. Wood, “On design and characterization of a soft multi-axis force sensor using embedded microfluidic channels,” *Sensors J.*, vol. 10, no. 10, pp. 4056–4064, 2013.
- [4] J. Lee, S. Kim, J. Lee, D. Yang, B. C. Park, S. Ryu, and I. Park, “A stretchable strain sensor based on a metal nanoparticle thin film for human motion detection,” *Nanoscale*, vol. 6, no. 20, pp. 11932–11939, 2014.
- [5] N. Lu and S. Yang, “Mechanics for stretchable sensors,” *Curr. Opin. Solid State Mater. Sci.*, vol. 19, no. 3, pp. 149–159, 2015.
- [6] Y. L. Park, B. Chen, and R. J. Wood, “Design and fabrication of soft artificial skin using embedded microchannels and liquid conductors,” *IEEE Sensors Conf.*, vol. 12, no. 8, pp. 2711–2718, 2012.
- [7] M. Amjadi, A. Pichitpajongkit, S. Lee, S. Ryu, and I. Park, “Highly stretchable and sensitive strain sensor based on silver nanowire-elastomer nanocomposite,” *ACS Nano*, vol. 8, no. 5, pp. 5154–5163, 2014.
- [8] N. Lu, C. Lu, S. Yang, and J. Rogers, “Highly sensitive skin-mountable strain gauges based entirely on elastomers,” *Adv. Funct. Mater.*, vol. 22, no. 19, pp. 4044–4050, 2012.
- [9] D. Kang, P. V. Pikhitsa, Y. W. Choi, C. Lee, S. S. Shin, L. Piao, B. Park, K. Y. Suh, T. I. Kim, and M. Choi, “Ultrasensitive mechanical crack-based sensor inspired by the spider sensory system,” *Nature*, vol. 516, no. 7530, pp. 222–226, 2014.

- [10] M. Park, J. Im, M. Shin, Y. Min, J. Park, H. Cho, S. Park, M. B. Shim, S. Jeon, D. Y. Chung, J. Bae, J. Park, U. Jeong, and K. Kim, "Highly stretchable electric circuits from a composite material of silver nanoparticles and elastomeric fibres," *Nat. Nanotechnol.*, vol. 7, no. 12, pp. 803–809, 2012.
- [11] C. X. Liu and J. W. Choi, "Patterning conductive PDMS nanocomposite in an elastomer using microcontact printing," *J. Micromechanics Microengineering*, vol. 19, no. 8, 2009.
- [12] J.-B. Chossat, Y.-L. Park, R. J. Wood, and V. Duchaine, "A Soft Strain Sensor Based on Ionic and Metal Liquids," *IEEE Sens. J.*, vol. 13, no. 9, 2013.
- [13] A. Tabatabai, A. Fassler, C. Usiak, and C. Majidi, "Liquid-phase gallium-indium alloy electronics with microcontact printing," *Langmuir*, vol. 29, no. 20, pp. 6194–6200, 2013.
- [14] T. Liu, P. Sen, and C. J. Kim, "Characterization of nontoxic liquid-metal alloy galinstan for applications in microdevices," *J. Microelectromechanical Syst.*, vol. 21, no. 2, pp. 443–450, 2012.
- [15] T. Yamada, Y. Hayamizu, Y. Yamamoto, Y. Yomogida, A. I. Najafabadi, D. N. Futaba, and K. Hata, "A stretchable carbon nanotube strain sensor for human-motion detection," *Nat. Nanotechnol.*, vol. 6, no. 5, pp. 296–301, 2011.
- [16] S. Agarwala, G. L. Goh, Y. L. Yap, G. D. Goh, H. Yu, W. Y. Yeong, and T. Tran, "Development of bendable strain sensor with embedded microchannels using 3D printing," *Sensors Actuators, A Phys.*, vol. 263, pp. 593–599, 2017.
- [17] J. H. Kong, N. S. Jang, S. H. Kim, and J. M. Kim, "Simple and rapid micropatterning of conductive carbon composites and its application to elastic strain sensors," *Carbon*, vol. 77, pp. 199–207, 2014.